

In flow magnetophoresis

Explorative research towards a cancer watch

Master thesis by: Tom Niessink

Date: 26-8-2021

Committee members:

Prof. Dr. Leon Terstappen, MD.

Prof. Dr. Ir. Mathieu Odijk

Ir. Michiel Stevens

University of Twente, the Netherlands

Page intentionally left blank

Voorwoord

Enschede, augustus 2021

Kanker is een ziekte die mijn familie al voor mijn geboorte getekend heeft, allereerst door het overlijden van mijn grootmoeder op 48 jarige leeftijd. Later verloor ik helaas ook mijn beide grootvaders aan de ziekte. Tijdens mijn middelbare schooltijd verloor ik eerst opa Bert aan longkanker en daarna in het begin van mijn studententijd overleed opa Gerrit aan acute leukemie.

Kankerpatiënten worden vaak doodziek van hun behandeling en moeten daarna weken of soms zelfs maanden wachten om te horen of deze aanslaat. Deze spanning is voor de patiënt en hun familie ondragelijk. Het is dan ook geweldig dat de Cancer Watch hier misschien al tijdens de behandeling zelf uitsluitsel over kan geven.

Ik hoop vooral dat het werk dat ik hier presenteer Leon en Michiel verder kan helpen met hun project. Ik vond het een waar plezier om hier aan bij te kunnen dragen en ik zal er zeker met gepaste trots naar terugkijken, vooral wanneer ooit de eerste patiënten aangesloten worden op de Cancer Watch.

Tom Niessink (nu nog Bsc.)

Summary

Circulating Tumor Cells (CTC's) are highly valuable for cancer diagnostics. Terstappen et al. proposed a wearable device called Cancer Watch which will be able to retrieve these cells in a dialysis-like manner. A present day alternative is offered by diagnostic leukapheresis (DLA), which filters nucleated cells, including CTC's from circulation.

In this thesis, a new microfluidic platform for processing DLA is explored. This platform consist of two steps:

1. A rough immunomagnetic separation, which will reduce the volume of the sample and perform a first purification step.
2. A fine immunomagnetic separation, which will sort the sample into fractions with different EpCAM expression.

The rough separation was tested with Ibidi μ -slides using MATLAB and COMSOL simulations and experiments with cells in buffer. An Ibidi slide with a height of 600 μm was found to be optimal, together with a flow rate of 0.5 ml sample per min. As for the magnet used for attracting the cells, an optimized Halbach array consisting of $1 \times 2 \times 12 \text{ mm}^3$ and $1 \times 2.75 \times 12 \text{ mm}^3$ N52 magnets was shown to outperform all other available configurations. Unbound cells could be washed effectively by flowing 2-4 ml of buffer at a flow rate of 1-2 ml/min through the channel. There were no limits in throughput discovered and the process could be performed with 3 chips in parallel, which decreased processing time but slightly lowered recovery.

For the fine separation, a specialized chip was designed with the use of COMSOL and then micro milled in PMMA. A total of 3 iterations lead to the production of a chip which could effectively deflect LNCAP, PC3 and PC3-9 cells into different groups based on their magnetic moment. This deflection was evaluated using microscopy, which showed a good separation of fractions. At the moment however it is not possible to retrieve these populations from the chip. It was possible to perform particle image velocimetry with the chip, which was used to evaluate the magnetic moment of cells. This was applied to evaluate magnetic properties of three types of ferrofluids, of which CellSearch VU1D9 ferrofluid showed highest results.

Keywords: Circulating Tumor Cells, Microfluidics, Immunomagnetic Separation

Content

Voorwoord	3
Summary	3
1. Introduction	6
1.1 Context.....	6
1.2 Problem statement	7
1.3 Thesis outline	8
2. Rough Separation.....	9
2.1 Introduction	9
2.2 Method.....	10
2.2.1 Physics	10
2.2.2 Finite differences & Monte Carlo Modelling.....	13
2.2.3 Experimental	14
2.3 Results	18
2.3.1 Modelling	18
2.3.2 Experimental	19
2.4 Discussion	24
2.4.1 Optimizing flow conditions	24
2.4.2 Finding the optimal magnetic array	24
2.4.3 Removing unbound cells	25
2.4.4 Investigating limits in throughput.....	25
2.4.5 Use of parallel processing.....	25
2.5 Conclusion.....	26
3. Fine separation	27
3.1 Introduction	27
3.2 Method.....	28
3.2.1 COMSOL modelling.....	28
3.2.2 Chip production.....	29
3.2.3 Experimental testing	32
3.3 Results	38
3.4 Discussion	47
3.4.1 Flow focusing.....	47
3.4.2 Magnetic configuration.....	47
3.4.3 Cell sorting based on magnetic moment.....	49
3.4.4 Particle image velocimetry for measuring magnetic moment.....	49

3.5 Conclusion.....	49
4. The clinical perspective.....	50
4.1 Diagnostic Leukapheresis Product.....	50
4.2 Towards a Cancer watch.....	51
5. Recommendations.....	53
5.1 Rough separation.....	53
5.2 Fine separation.....	53
6. Acknowledgements.....	55
7. Resources.....	56
Appendix A: Supplementary to physics.....	59
A.1 Derivation of the flow field.....	59
A.2 Extra information on formulas used in MATLAB script.....	60
Appendix B: Supplementary to MATLAB simulations.....	61
B.1 Spread of magnetic moment.....	61
B.2. Modelling the magnetic field in COMSOL.....	62
Appendix C: validation of MATLAB based cell counting.....	63
Appendix D: Additional results to chapter 2.....	64

1. Introduction

1.1 Context

The widely diverse nature of cancer makes choosing the optimal treatment very complex [1]. Traditionally, treatment protocols were guided by the result of cohort based studies, making conclusions at the level of populations rather than individuals [2, 3]. Patients however have many different characteristics, making them a very heterogeneous population. Personalized medicine is a treatment method in which therapy choices are guided by patient specific properties [2, 3]. Instead of treating a whole population of similar patients with the same therapy, knowledge of patient specifics, such as genetic mutations are used to choose more targeted and effective treatments [4, 5].

The application of patient specific treatments require patient specific knowledge. Circulating Tumor Cells (CTCs) have the potential to offer this kind of information. CTC's are cells in blood circulation which originate from tumor tissue [6] The number of CTC's per ml of blood shows very strong correlation with disease progression, treatment effectiveness and overall patient survival [7-9]. Isolated CTC's can also be used for genetic characterization [9-12]. The occurrence of CTC's is low, with typical incidence rates of 1-10 cells per ml of blood in patients with metastatic carcinoma's [13]. This makes collecting these cells a rather difficult task. Multiple methods are commercially available for CTC enrichment, including filtration, density gradient separation or immunologic [11, 13, 14]. Among these, EpCAM based immunomagnetic enrichment (the CellSearch method) is the only one currently approved for clinical practice by the FDA. This method uses 7.5 ml whole blood samples to enrich CTCs from, which is low invasive and can therefore be performed often without much hindrance to patients.

The rarity of CTC's and the sensitivity of downstream analysis methods call for a new method to gather much more of these cells. Terstappen et al. proposed a wearable device (or 'Cancer Watch') which will capture magnetically labeled CTC's directly from blood circulation. Blood will continuously flow through the device, where it is incubated with immunomagnetic nanoparticles. Then, magnets will be used to capture the valuable CTC's while leaving erythrocytes and leukocytes in circulation (Figure 1).

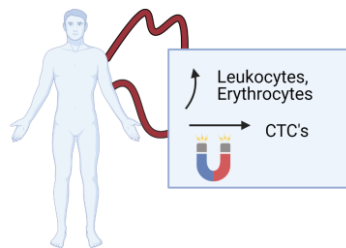


Figure 1: The principle of a Cancer Watch. CTC's remain trapped in the device while leukocytes and erythrocytes remain circulating. Ideally, such a device would be wearable.

Unfortunately, despite of research into its development, the use of such a device is still science fiction. A present-day alternative is offered by Diagnostic Leukocyte-Apheresis (DLA). Using density differences, the complete mononuclear cell fraction of a patient is retrieved from blood circulation in a dialysis-like manner. As they are similar in density to leukocytes, CTC's will end up in this fraction [15, 16]. This method significantly increases the amount of CTC's in the sample [17]. Processing DLA samples using the standard CellSearch method used for whole blood proves to be problematic however, as both the size of the sample and the concentration of leukocytes is much higher [16]. Other techniques to process DLA have been attempted, including filtration and immunologic leukocyte depletion but further improvements are still required to truly reach the full potential of DLA [16]. This thesis will attempt to work towards a novel method for DLA enrichment and explore techniques which can later be used in a Cancer watch.

1.2 Problem statement

The processing of DLA towards a product that can be used for downstream analysis poses two specific challenges:

- The ability to process large amount of sample within the course of a few hours
- The ability to reduce the number of leukocytes in a DLA sample from several billion to several hundreds of cells

In this thesis, a new method will be proposed to tackle these challenges with a two step method (Figure 2). DLA product, which is already incubated with anti-EpCAM ferrofluids, will first be processed using a 'rough' separation. This will decrease the size of the sample and increase purity. This will be followed by a 'fine' separation. Here, cells are sorted into fractions based on their magnetic attraction, which is related to EpCAM expression.

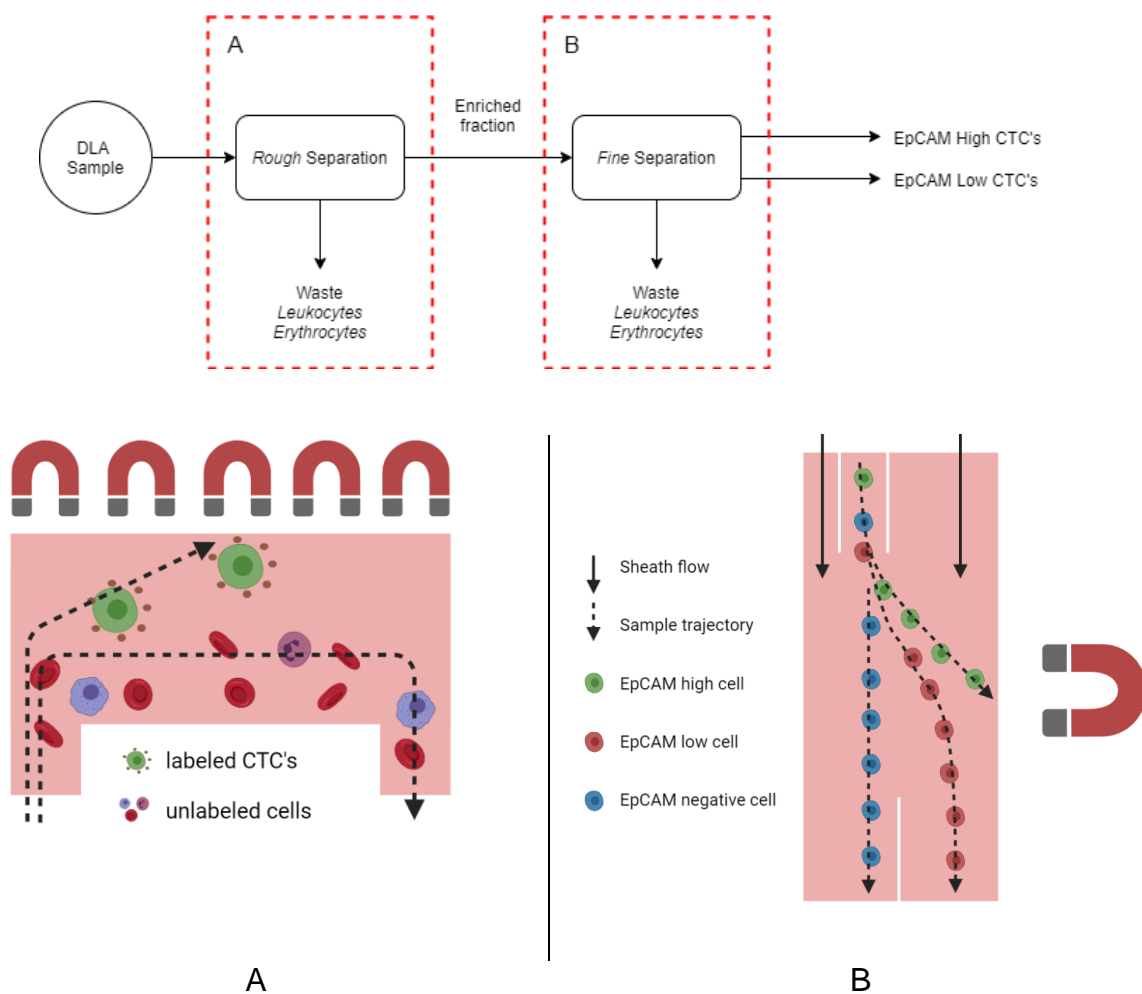


Figure 2: The proposed separation system. First, a rough separation is performed, using the principle shown in A. The enriched fraction is then retrieved and processed using the Fine separation, which is shown in B.

Both the rough and fine separation will be performed using flow-based microfluidic systems. For the rough separation, commercially available Ibidi μ -slides will be utilized. These microchips consist of a channel in the range of 200-800 μm and have a very thin bottom plate, allowing the magnet to be placed close to the channel.

In the fine separation, cells are flown through a sorting channel in a thin stream. A magnet will be placed to attract cells from this stream. As there currently is no platform available to perform these kind of separations, a specialized chip will be produced. This chip will be evaluated using experiments and COMSOL modelling and based on these results, design reiterations will be performed. The final design will be tested experimentally.

Following the statements above, two sets of research questions have been determined, addressing the specific parts of the separation process.

Rough separation

- What combination of flow rate and channel height leads to an optimum in recovery for CTC enrichment with Ibidi μ -slides?
- What is the optimal magnetic configuration for CTC enrichment in Ibidi μ -slides?
- What is the optimal flow rate and buffer throughput for removing unbound cells from the separation channel?
- Are there limits in sample throughput for the rough separation using Ibidi μ -slides?
- Is it possible to process sample through multiple slides in parallel?

Fine separation

- How can a magnetic cell sorting device be produced?
- How can cells be focused in a narrow stream in the sorting device?
- What is an optimal magnetic configuration to sort cells with the device?
- Is it possible to calculate a measure of magnetic properties of cells based on the deflection of cells in the sorting device?

1.3 Thesis outline

In chapter 2, MATLAB-, COMSOL- and experimental models will be used to optimize immuno-magnetopheresis according to the rough separation principle. The questions above will be answered and an optimized protocol will be established. In chapter 3, COMSOL will be utilized to design a magnetic cell sorting device, which is then built and tested experimentally. Several re-iterations of the design are made towards a functional sorting device. In chapter 4, the results of chapters 2 and 3 are put into a clinical perspective; how can the work which is performed be applied for use with DLA product and how does this bring us closer towards an operable Cancer Watch? Chapter 5 contains some recommendations on how this project can be continued.

2. Rough Separation

2.1 Introduction

The goal of the rough separation is to have a high sample throughput combined with a high recovery of CTC's. The principle of using microfluidics for immunomagnetophoresis has been shown to work with cell lines by Hoshino et al (2011, [18]), who found a 86% recovery for SKBR-3 cells spiked in whole blood, with a sample throughput of 10 ml/hour. They used a PDMS channel with a glass bottom and three large block magnets which were placed in parallel with the channel (Figure 3).

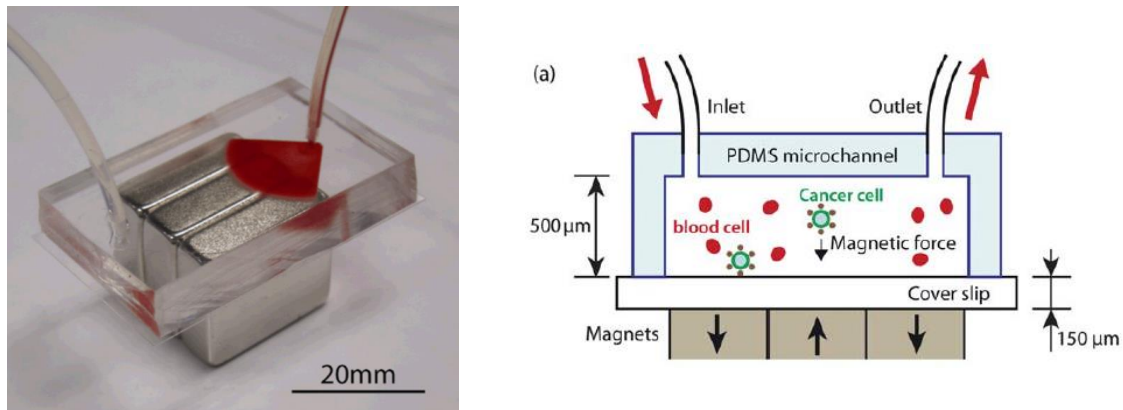


Figure 3: The magnetophoresis device produced by Hoshino et al. Image on the left shows a photograph, image on the right shows a schematic depiction of their device. Images taken from their 2011 paper [18].

A similar setup will also be used for the rough separation. DLA product can be over 60 ml of sample, thus the throughput should be increased quite some to make the setup feasible for practical use. Factors including channel dimensions, flow rate and magnetic configuration should be optimized [19]. These are strongly connected to each other, which makes optimization a complex process. An optimized protocol will have the highest recovery possible for a reasonable processing time.

Creating a high magnetic field gradient is a factor that can improve recovery [20]. The use of smaller magnets will decrease the outreach of the field but increase the gradient, especially close to the surface of these magnets. Halbach arrays are special magnet configurations which are built such that the magnetic field gradient is forced out of the magnet array, increasing the outreach. A Halbach array of small magnets will therefore have a large magnetic field gradient with a relatively large outreach, which should be beneficial for recovery [21].

One of the advantages of a flow based system is its independency of sample size. However, with each ml of sample more particles and cells collect in the channel. Using a standard incubation concentration of 3.3 $\mu\text{g/ml}$, processing a full 60 ml DLA sample will lead to the collection of $\sim 200 \mu\text{g}$ of ferrofluid. This iron might influence the magnetic field in two ways. On one hand, the particles themselves will be magnetized, creating their own small additional magnetic field [20]. This will increase the magnetic force on cells which are already captured. On the other hand, over larger distances, this presence of iron might decrease the magnetic field. This effect is called magnetic shielding and is utilized for protection of all kinds of sensitive electronics, for example in aviation [22].

2.2 Method

2.2.1 Physics

To be able to simulate the trajectories of cells in the channel we need to establish which physics play a role in the immunomagnetic separation process. Cells in the channel are influenced by multiple forces, including gravity, buoyancy, drag and magnetic attraction forces (Figure 4) [19]. Drag force on a cell can either be positive or negative, depending on the velocity of the cell relative to the medium. Magnetic attraction forces are directed towards the magnet and are the forces that enable magnetophoresis. Gravity, buoyancy and other forces like lift-forces are considered negligible within the used dimensions and timespan [19].

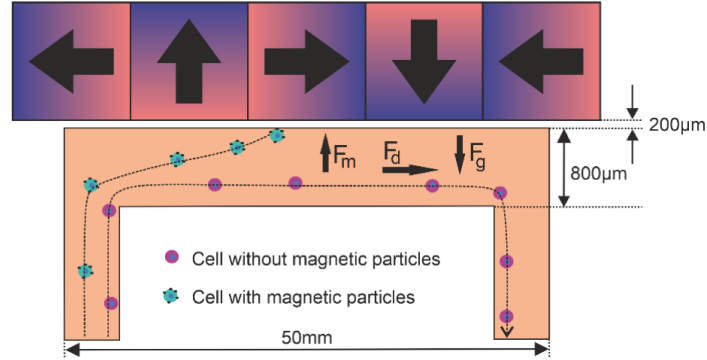


Figure 4: Forces on a cell in flow. Drag force can be directed in either way, depending on the velocity of the cell relative to that of the medium. Image from [21].

Describing flow in the channel

We need to be able to calculate the flow profile of the channel if we want to simulate the microfluidic device. Assuming that the flow in the channel behaves as a flow rate driven, laminar, Hagen-Poiseuille flow, the flow speed at a certain height in the chamber can be found with formula (1). This formula is based on Bruus et al. [23] and its derivation is available in appendix A.1.

$$v(x) = \frac{3}{4}(x^2 - a^2) \frac{LQ}{a^3w} \quad (1)$$

In this formula is $v(x)$ the flow speed (m/s) on a certain location in the channel x (m), a half the channel height (m), L the channel length (m), Q the flow rate (m³/s) and w the channel width (m).

Forces acting on the cells

We only consider two kinds of forces acting on cells in the channel, drag force and magnetophoretic force. For now we assume that magnetic attraction only occurs in vertical direction, perpendicular to the flow. The flow will exert drag force on the cells. The formula for drag force is [18]:

$$F_d = 6\pi\eta R(v_{\text{medium}} - v_{\text{cell}}) \quad (2)$$

With η the viscosity of the medium (Pa/s), R the cellular radius (m) and v_{cell} , v_{medium} the velocities of the cells and the medium they are in (m/s). Because there are no counteracting forces in horizontal direction, we assume that the drag force is to such an extent that the acceleration of the cell to terminal velocity ($v_{\text{medium}} = v_{\text{cell}}$) happens instantly or has taken place before entering the simulated area. This means that the velocity of a cell is equal to the flow profile. In vertical direction, two forces are counteracting. The drag force (eq 2) and the magnetophoretic force [21]:

$$F_{\text{mag}} = \frac{\mu_0}{2H} \mathbf{m}(\mathbf{H}) \nabla(\mathbf{H}^2) \quad (3)$$

With μ_0 the magnetic permeability of vacuum (N/A^2), $\mathbf{m}(\mathbf{H})$ the magnetic moment of the cell (Am^2) and \mathbf{H} the magnetic field (A/m). The magnetic moment $\mathbf{m}(\mathbf{H})$ is on itself dependent on the magnetic field. It can be defined as:

$$\mathbf{m}(\mathbf{H}) = f(\mathbf{H}) \cdot m_{\text{sat}} \quad (4)$$

Where,

$$f(\mathbf{H}) = \begin{cases} \sqrt{\sin\left(\frac{\mathbf{H}}{H_{\text{max}}} * \frac{\pi}{2}\right)} & \text{if } \mathbf{H} < H_{\text{max}} \\ 1 & \text{if } \mathbf{H} \geq H_{\text{max}} \end{cases} \quad (5)$$

With m_{sat} being the magnetic moment of the cell when the magnetization of the ferrofluids is to such an extent that all particles are saturated (Am^2), and H_{max} the value of the field at which saturated magnetization is reached. This leads to equation (6)

$$F_{\text{mag}} = \frac{\mu_0}{2H} f(\mathbf{H}) \cdot m_{\text{sat}} \nabla(\mathbf{H}^2) \quad (6)$$

Particles attracted by a magnet do not accelerate indefinitely but will have a terminal velocity. At this velocity, there is no resultant force, thus $F_{\text{mag}} = F_{\text{drag}}$.

$$\frac{\mu_0}{2H} f(\mathbf{H}) \cdot m_{\text{sat}} \nabla(\mathbf{H}^2) = 6\pi\eta R(v_{\text{medium}} - v_{\text{cell}}) \quad (7)$$

The medium is moving in horizontal direction and it is stationary in vertical direction. Therefore, v_{medium} is equal to zero. Rewriting equation 7 gives:

$$v_{\text{cell}} = -\frac{\frac{\mu_0}{2H} f(\mathbf{H}) \cdot m_{\text{sat}} \nabla(\mathbf{H}^2)}{6\pi\eta R} \quad (8)$$

Which is an expression for velocity in vertical direction. To attract cells effectively, the horizontal velocity should be as low as possible while the attraction towards the magnet should be as high as possible. Decreasing the horizontal velocity is relatively easy but limits the sample throughput rate. When we assume that we can't change the medium viscosity or change the size of the cells, the attraction towards the magnet can be increased in two ways:

- Increase m_{sat}
- Increase $\nabla\mathbf{H}^2$

There are multiple methods to increase m_{sat} , including specialized ferrofluid incubation techniques [24]. Also it is possible to enhance the magnetic properties of the ferrofluid [20]. Optimization of these techniques is interesting and is being performed but is not within the scope of this thesis. $\nabla\mathbf{H}^2$ however can be increased by using magnet arrays optimized for high gradients.

Captured cells

While the model thus far describes the physics behind the trajectory in the channel, it does not account for cells which are captured on the bottom. On the channel wall, drag force is equal to zero but there will be a shear stress which deforms and moves cells ([19]). In this thesis, we will not try to calculate the effect of shear stress on the cells but we will try to find how magnetic cells must be to be retained in a known magnetic field. Equation (9) describes the shear stress due to a fluid flow in a rectangular channel [23]:

$$\tau(x) = \frac{F_{\text{shear}}}{A} = \eta \frac{\partial v(x)}{\partial x} \quad (9)$$

With F_{shear} being the force due to shear (N), A the area (m^2), η viscosity ($\text{Pa}\cdot\text{s}$), and $v(x)$ the flow profile in the channel (m/s), which is described in equation (1). Filling in and differentiation leads to equation (10):

$$\tau(x) = \eta \frac{6LQ}{4a^3w} x \quad (10)$$

As stated before when describing equation (1), L is defined as the length of the channel (m), Q as the sample rate (m^3/s), a as half the channel height (m) and w is the channel width (m). Using equations (9), and (10) we can find the shear force applied to a cell sized area, which is described in equation (11):

$$F_{\text{shear}} = \eta \left(\frac{6}{4} \frac{LQ}{a^3w} x \right) A \quad (11)$$

If we ignore friction between the wall and the cell, only the magnetophoretic force (equation (6)) will keep cells from flushing. To be able to retain cells the magnetophoretic force should at least be equal to the shear force:

$$F_{\text{shear}} = F_{\text{mag}} \quad (12)$$

Filling in equations (6) and (11) leads to equation (13):

$$\eta \left(\frac{6}{4} \frac{LQ}{a^3w} x \right) A = \frac{\mu_0}{2H} f(H) \cdot m_{\text{sat}} \nabla(H^2) \quad (13)$$

Which can be rewritten to equation (14):

$$m_{\text{sat}} = \frac{\eta \left(\frac{6}{4} \frac{LQ}{a^3w} x \right) A}{\frac{\mu_0}{2H} f(H) \cdot \nabla(H^2)} \quad (14)$$

Which describes the minimum magnetic moment a cell should have to overcome shear stress due to liquid flow in a known magnetic field gradient (∇H^2). This is related to the amount of ferrofluids bound to a cell.

2.2.2 Finite differences & Monte Carlo Modelling

To achieve better understanding of the rough separation process a model was built¹. This model utilized the finite differences method (FDM) to simulate the trajectories of cells in the channel. In finite differences, the value of a variable somewhere at a set difference from a known value is approximated using a Taylor series expansion. As we are interested in locations over time, we get two formulas, which we define as $X(t)$ and $Y(t)$, with X being the location on the horizontal axis (parallel to the magnets) and Y the vertical axis (perpendicular towards the magnet). This gives the two following first order Taylor series:

$$X(t + dt) = X(t) + X'(t) * dt \quad (14)$$

$$Y(t + dt) = Y(t) + Y'(t) * dt \quad (15)$$

As X' is the displacement in horizontal direction, it is equal to equation 1. Y' is the displacement in vertical direction and equal to equation 8. The definition used in the simulation is derived from this equation, which is described in appendix A.2.

For each simulated cell a magnetic moment and a starting position in the channel was randomly generated from distributions around the average values of both variables. By performing many iterations an accurate estimation of the situation can be reached. This method of modelling is called the Monte Carlo method and it is widely applied in physics, economics and engineering when simulating problems with uncertain starting conditions. For this model, PC3-9 cells were simulated with a maximum magnetic moment of $9.2E-14 \text{ Am}^2$ [25] and a distribution of 220% CV (appendix B.1). The magnetic field was be modelled using COMSOL (appendix B.2) and transferred to MATLAB. For each configuration, 6000 iterations were performed. These iterations were divided into groups of 120 cells of which an recovery rate and standard deviation was calculated. This was done to better approach the actual experiments, which also consists of small batches of cells being separated.

¹ The complete MATLAB simulation software is available on GitHub and accessible via: <https://github.com/TomNiessink/SimulationCellTrajectories>

2.2.3 Experimental

2.2.3.1 Setup

For the separation channel, μ -slides were purchased from Ibidi (cat#80176) with channel heights of 0.2, 0.4, 0.6 and 0.8 mm. These chips have Leur inlets and have a surface of 5x50 mm². There were two configurations used for the experiments on rough separation, visible in Figure 5. In both cases, cells are drawn from the sample tube to the pump. In setup 1, the collected cells are flushed back into the sample channel, while in setup 2 the cells are flushed into an additional collection tube. The flushing is performed by sequentially flushing 1 ml air – 1 ml buffer – 1ml air – 1 ml buffer – 1ml air.

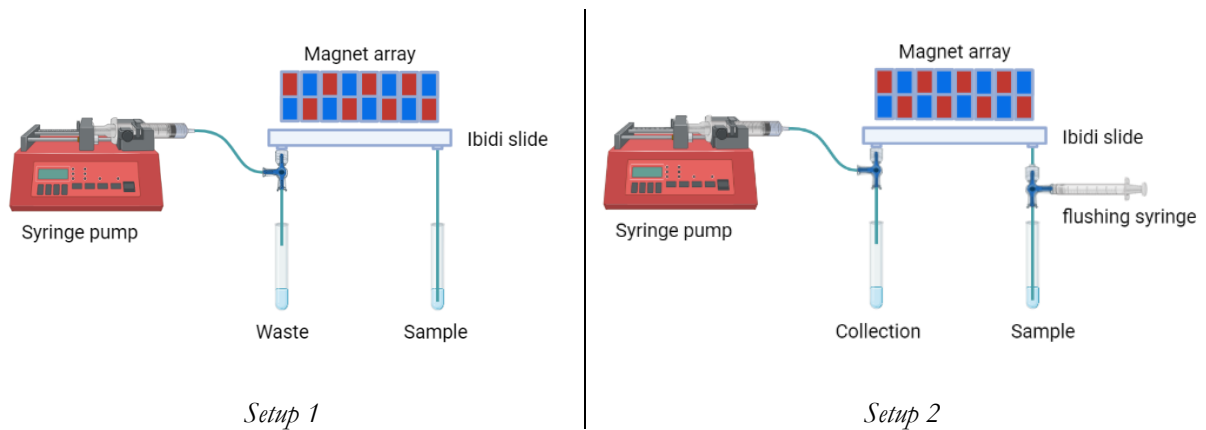


Figure 5: Schematic depiction of the two setups used in experimental testing. Both setups use negative pressure to pull the sample through the chip. The main difference between the two setups is that in setup 1, the enriched sample is flushed with air coming from the syringe pump back in to the sample inlet, and with setup 2 the enriched sample is flushed with an additional flushing syringe into a special collection outlet.

To prevent cells from clinging to either the tubing or the channel walls, the setup was treated with casein buffer for at least 15 minutes for every use. This buffer is commonly used as a blocking agent in immunochemistry protocols [26] and should therefore block possible sites for the cells to bind to.

In the following experiments, five different cell lines were used. All cell lines were cultured under standard conditions and were fixed using 1% formaldehyde before use. LCL and THP-1 cells were used as a substitute for leukocytes, and were considered EpCAM negative. PC3 cells and PC3-9 cells were considered to be EpCAM low cells, with average EpCAM expressions of 7000 molecules for PC3 cells and 20000 molecules for PC3-9 cells. LNCAP cells were considered to be EpCAM high, with an average expression of over 630 000 molecules per cell.

2.2.3.2 Optimizing flow conditions

All available sizes of Ibidi slides were tested to find the optimal channel height. To find the optimal flow rates, flows of .5 ml/min, 1 ml/min, 1.5 ml/min and 2 ml/min were tested on each chip. Setup 1 was used for each measurement, with a North-South (alternating orientation) array of 3x12x15 and 4x12x15 mm N52 magnets.

For this experiments, PC3-9 cells stained with CellTracker Orange were incubated with .3 $\mu\text{g}/\text{ml}$ of VU1D9 ferrofluid (Biomagnetic Solutions) for 3x10 min in a BD iMag Cell Separation Magnet (from hereon called BD magnet Array). Around 150 cells were pipetted in four to five droplets on a microscope slide, imaged and counted using a MATLAB script for automatic cell counting². Then, cells are rinsed into a FACS tube using 2 ml of casein buffer and flown through the system. Separated cells were flushed out and were collected on a 24 well plate. The collected samples were stored overnight and counted the day after on a NIKON Eclipse TI inverted fluorescence microscope.

To investigate what is happening when cells are captured in the channel, 10 000 of those PC3-9 cells were captured in a 800 μm channel. With the North-South magnet array attached, these cells were sequentially washed with 1 ml of casein buffer using increasing flow rates. During washing, in- and outflux of cells which were captured on a gradient line (the area between two magnets where the gradient is highest) was filmed using a Nikon fluorescence microscope. This way, the movement of cells between the gradient lines was investigated. Produced video's were manually reviewed and processed in ImageJ.

2.2.3.3 Optimizing magnet setup

When the optimal flow conditions were known, the optimization could proceed by finding the right magnetic configuration. Using COMSOL Multiphysics 5.3, an optimized magnetic Halbach array was designed [21]. The optimized Halbach array consisted of two types of magnets; 1x2x12 mm³ N52 magnets which were oriented horizontally and 1x2.75x12 mm³ N52 magnets which were oriented vertically. This was compared to an array of 1x1.5x5 mm³ N45 magnets which were placed in 3 rows and an array of 4x4x15 mm³ N45 magnets (Figure 6).

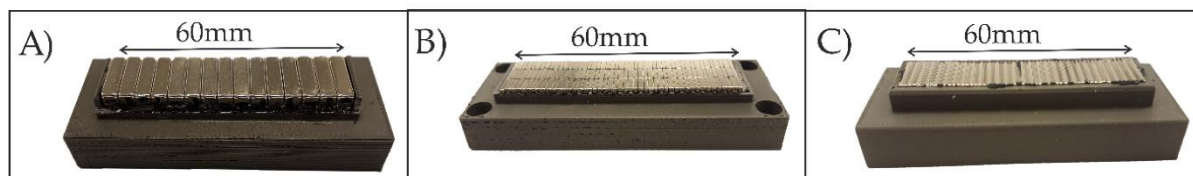


Figure 6: A) 4x4x15 mm³ N45 Halbach array, B) 1x1.5x5 mm³ N45 Halbach array, C) Optimized Halbach array.

PC3, PC3-9's and LNCAP cells were stained with different CellTracker dyes (CT Orange, CT Deep Red and CT Green) and Hoechst. A mixture of these colored cells (~40 000 of each type) was incubated with 15 μl CellSearch ferrofluids per ml of sample for 3x10 minutes in a BD magnet array. After washing away unbound ferrofluids, this sample was then divided into four fractions, three of those were used for testing the different configurations and one as a control. Setup 2 of Figure 5 (page 14) was used as a setup. A chip of 800 μm height was used, with a flow speed of 1 ml/min.

² The MATLAB script is based on threshold gated image segmentation. When compared to a 'golden' standard of manually counting from microscopic photos, the script had an accuracy of 95.2% in 15 photos. This validation is available in Appendix C. The MATLAB script is available on GitHub and accessible through: <https://github.com/TomNiessink/AutomaticCellCounter>

After flowing through the chip a washing step was performed by flowing 2 ml of clean buffer at a flow rate of 1 ml/min through the channel. Then, the sample was collected in a BD TruCount counting tube and counted using a BD FACSAria II flow cytometer. Cells were gated on cell size (Forward scatter, sideward scatter), nucleus and expression of the dye.

Besides processing these samples with the flow-through separation, a similar sample was also processed using the standard CellSearch method. The CellSearch profile kit without any staining was used. Samples were analyzed and counted with flow cytometry.

2.2.3.5 Removing unbound cells

To maximize leukocyte depletion, all unbound cells should be removed from the system. This process takes place in two steps: rinsing, which consist of flowing an additional amount of buffer through the sample tube at the separation flow rate to ensure that all sample has flown through and washing, which can be described as flowing clean buffer through the chip at higher flow rate to wash away unbound cells.

To investigate when a sample is rinsed properly, a 800 μm channel in Setup 1 was filled with buffer. Then, 1 ml of food coloring was flown through the channel. The waste was collected and the food coloring was then rinsed with an additional 1 ml of buffer. Again, waste was collected and an additional rinsing and collection step was performed. Using photo-spectrometry, concentration of food coloring was determined in each fraction.

To optimize washing, an additional experiment was performed, in which both specifically and unspecifically captured cells were washed with different flow rates of buffer. For this experiment, PC3-9 cells were stained with CellTracker Deep Red and LCL cells were stained with CellTracker Orange. 10 000 of these PC3-9 cells were incubated with 3.3 $\mu\text{g}/\text{ml}$ of CellSearch ferrofluid for 3x10 min in a BD array. After incubation, one million LCL cells were spiked into the sample. The sample was then separated using a 800 μm chip, the optimized Halbach array and a flow rate of .5 ml/min. Then, flow was reversed and cells were washed with (subsequentially) two ml of casein buffer at 1ml/min, 2ml/min, 4ml/min and 8ml/min. Each two ml fraction was collected in a counting tube. This was performed in triplo. An additional sample was made in which no magnetic separation was performed.

2.2.3.4 Investigating limits in throughput

With the flow conditions, magnetic setup and washing protocol all tested, a next logical step was testing the limits of the system; how much can be processed in one run? The collection of large amounts of ferrofluids in the channel might influence the capture efficiency due to the magnetic shielding effect.

To test the effect of magnetic shielding, an experiment was performed in which cells were captured in channels which were pre-saturated with ferrofluids. In this experiment, 60 000 PC3-9 cells were incubated with 3.3 $\mu\text{g}/\text{ml}$ of ferrofluids (CellSearch) and CT Deep Red. First, a 800 μm channel was pre-saturated with either 100 μg , 50 μg , 25 μg , 12.5 μg or 0 μg (control) of Biomagnetic Solutions streptavidin ferrofluids. Then 10 000 of cells were flown through each condition using Setup 2 of Figure 5 (page 14), a flow speed of 1 ml/min and the optimized 1x1 mm magnet array. Cells were collected in a BD counting tube and counted with flow cytometry.

A similar experiment was performed in which the channels were not only pre-saturated with ferrofluids but also with captured cells. Accordingly, LNCAP cells were stained with CT orange and then incubated with ferrofluids (BioMagnetic Solutions). A total of 4 tubes of LNCAPs were made: 20 000 LNCAP cells and 5 $\mu\text{g}/\text{ml}$ of ferrofluid, 40 0000 LNCAP cells and 10 $\mu\text{g}/\text{ml}$ of ferrofluid, 100 000 LNCAP cells and 25 $\mu\text{g}/\text{ml}$ of ferrofluid and 200 000 LNCAP cells and 50 $\mu\text{g}/\text{ml}$ of ferrofluid. Each tube was flushed through an 800 μm Ibidi chip using Setup 2 and the optimized array. 50 000 PC3-9 cells were incubated with 3.3 $\mu\text{g}/\text{ml}$ of ferrofluids (CellSearch) and CT Deep Red. 10 000 of these cells were flown

through each array. After washing, cells are collected in a BD counting tube and counted with flow cytometry.

To investigate dynamically how cells are flushed in and out the chip, cells with different colors were separated in sequence, such that it was visible when certain cells enter and leave the system. For this experiment, PC3-9 cells were stained with CT Orange, CT Deep Red and CT Green. 20 000 of each population was spiked in a different tube with 20 million LCL cells in 2ml of casein buffer and incubated with 3.3 $\mu\text{g}/\text{ml}$ of ferrofluid (CellSearch). Subsequently, the tube with CTO cells, the tube with CTDR cells and the tube with CTG cells were processed and labeled cells were magnetically separated. In between, waste was collected in BD counting tubes. The washing fraction and the separated fraction were also collected. This was compared to a similar experiment in which there were no LCL cells present.

2.2.3.5 Use of parallel processing

One method which can greatly reduce the processing time of large samples is processing with multiple chips in parallel. This way, a similar channel retention time can be kept with increased flow rates. To test this, three 600 μm Ibidi slides were placed in parallel as shown in Figure 7. To ensure a similar sample flowthrough in each chip, the tubing was placed such that each chip was connected to an equal length of tube.

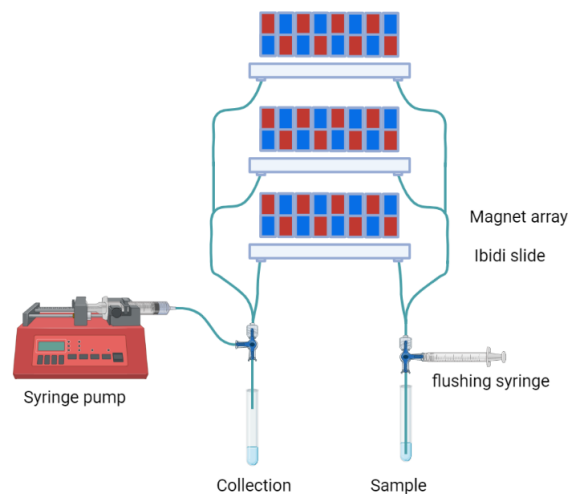


Figure 7: Schematic overview of the setup used to test processing with chips in parallel. In the actual situation, tubing was connected such that each chip was connected to a similar length of tubing, which ensures equal sample flowthrough.

To test this setup, roughly $\sim 15\,000$ LNCAP cells were stained with CTO and incubated for 3×10 min with 3.3 $\mu\text{g}/\text{ml}$ of CellSearch ferrofluids in a BD magnet array. After incubation, these cells were suspended in a volume of 10 ml Casein buffer and processed either with the parallel setup using a flow rate of 1.5 ml/min or using the normal situation with one chip and a flow rate of 0.5 ml/min. Recoveries were measured using flow cytometry.

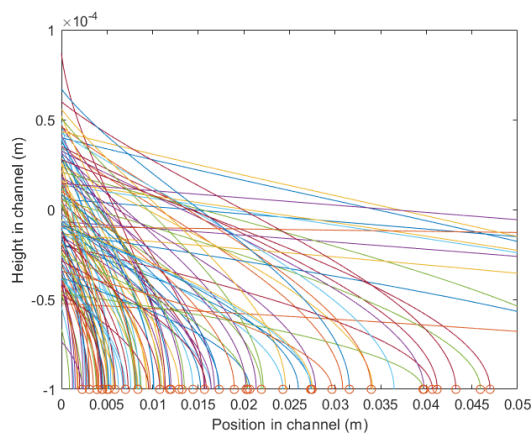
2.3 Results

2.3.1 Modelling

Simulated trajectories of cells flowing in a channel of $800\ \mu\text{m}$ in height with a flow rate of $.5\ \text{ml}/\text{min}$ are shown in Figure 8a. It is visible that cells can have very different trajectories, depending on their starting position and their magnetic moment. Cells with higher magnetic moments have steeper trajectories and being captured more upstream than cells with lower magnetic moments.

Figure 8b shows the results of all simulations performed with MATLAB. Some trends are quite clear. It is visible that for the same flow rate, an increase in channel height leads to a small decrease in recovery. An increase in flow rate however leads to a much larger decrease in recovery. With the same average flow velocity (the diagonal axes from lower left to upper right in Figure 8b), an increase in channel height will lead to a decrease in recovery.

The use of smaller channels both increases the average magnetic attraction and decreases the distance cells have to traverse, leading to a higher performance for smaller channels. For a fixed flow rate however a decrease in channel height will increase the average flow velocity and will lower the retention time, which counters a portion of the beneficial effects of the lower channels.



a. Trajectories of cells in a channel in one iteration of a simulation. The simulated channel was $800\ \mu\text{m}$ in height and a flow speed of $.5\ \text{ml}/\text{min}$ was simulated. Flow direction is from left to right.

Simulated recoveries (%)				
	$.5\ \text{ml}/\text{min}$	$1\ \text{ml}/\text{min}$	$1.5\ \text{ml}/\text{min}$	$2\ \text{ml}/\text{min}$
800 μm	86 ± 3	72 ± 3	60 ± 5	49 ± 4
600 μm	87 ± 3	75 ± 4	62 ± 4	54 ± 4
400 μm	88 ± 2	76 ± 4	65 ± 5	55 ± 4
200 μm	88 ± 3	78 ± 3	68 ± 4	58 ± 4

b. Table showing the results of simulating recoveries with different channel heights (vertical) and flow rates (horizontal), together with the standard deviation of these simulations ($n=50$)

Figure 8: Results of Monte-Carlo simulations of the different flow configurations. Simulations are performed within MATLAB.

2.3.2 Experimental

2.3.2.1 Optimizing flow conditions

Experimentally determining the optimal flow conditions lead to different results than modelled. The results of the optimization experiment is shown in Table 1. A more extensive version is available in appendix D. A graphical comparison between the model and the experiments is shown in Figure 9.

While in the simulated data smaller channels perform slightly better than larger channels, in the experimental data as shown in Table 1 it is clearly visible that there is an optimum in recovery for a 600 μm channel with a flow rate of .5 ml/min. In both cases however, lower flow rates perform better than higher flow rates, although in the experimental data this effect seems to decline with the larger channels.

Experimental recoveries				
Channel height	0.5 ml/min	1 ml/min	1.5 ml/min	2 ml/min
200 μm	59.0 \pm 11.8 %	36.7 \pm 17.5 %	38.7 \pm 4.2 %	31.7 \pm 10.1 %
400 μm	65.3 \pm 8.8 %	42.3 \pm 13.6 %	43.3 \pm 11.9 %	36.0 \pm 4.9 %
600 μm	85.7 \pm 12.5 %	48.7 \pm 11.1 %	44.3 \pm 5.7 %	41.0 \pm 16.4 %
800 μm	69.7 \pm 13.5 %	67.0 \pm 7.3 %	54.3 \pm 8.7 %	37.3 \pm 3.1 %

Table 1: Results of experimentally determining the optimum flow conditions for immunomagnetic separation with Ibidi chips. Shown are recovery rates of spiked PC3-9 cells in 2 ml samples.

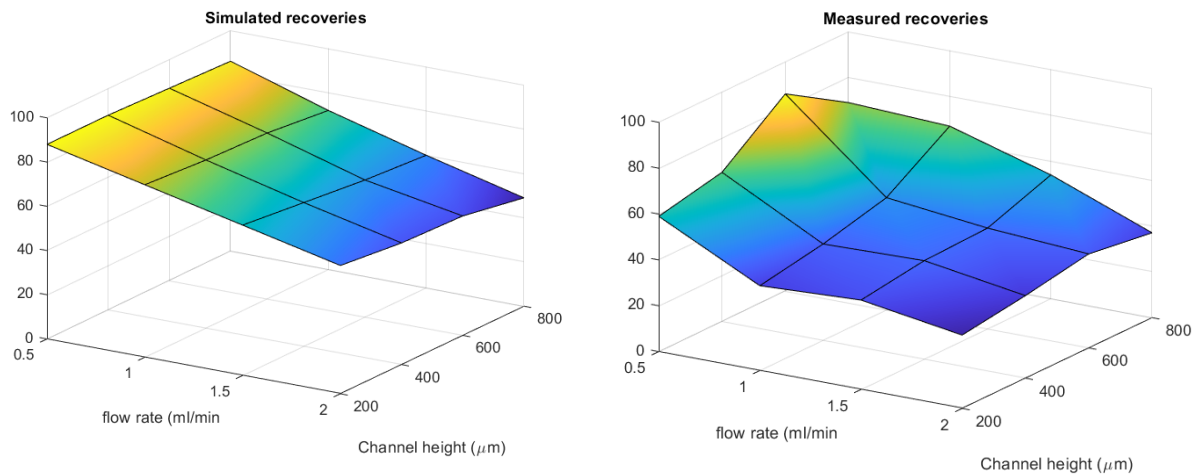


Figure 9: Simulated versus measured recoveries. Data is also available in Figure 8b for simulated and Table 1 for measured experiments. Z axis represents percentual recoveries.

While knowing the optimal flow rate and channel dimensions for recovery does answer the practical question on which configuration to use, the results also shows an inadequacy in the built model. One limit of the model is that the simulation stops when a cell has reached the bottom wall and it is assumed that there is no movement after.

The experiment in which captured PC3-9 cells were washed with different flow rates while being imaged under a microscope clearly shows that this assumption is incorrect, especially for the larger flow rates. Instead of being immobile, cells seem to move from gradient line to gradient line. Figure 10 shows an overlay of two photos, one made before and one made after washing at 7 ml/min. It is clearly visible that cells have moved between the two photographs. In Figure 11, it is visible how the flow speed of the buffer in the channel influences the ratio of movement of cells between magnetic gradient lines. It is clear that the amount of movement is not only dependent on the flow ratio, but also on the location in the channel, as the outflux of cells has a different peak in change than the influx. The amount of influx shows the movement of cells which were captured upstream.

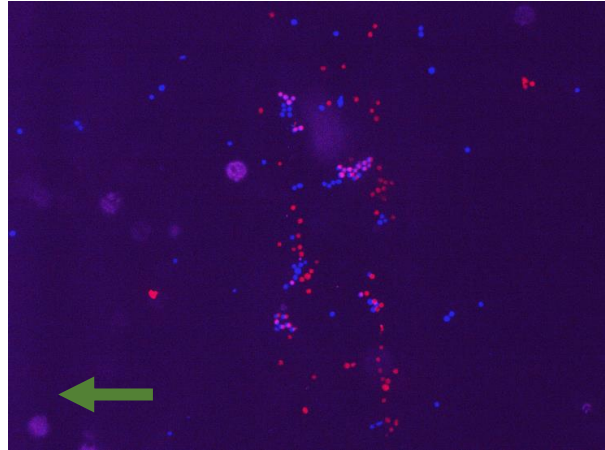


Figure 10: Overlay of before (red) and after (blue) photos of washing with 1 ml of buffer at 7 ml/min. Light purple cells have not moved during washing. It is visible that a large number of cells have moved during washing. Green arrow shows direction of flow.

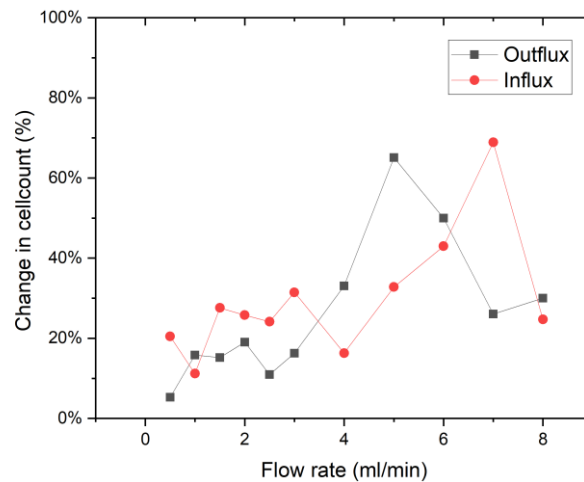


Figure 11: Counted in- and outflux of cells due to washing at different flow rates. Cells were captured in a 800 μm Ibidi slide using a North-South oriented magnet array. Visible are two clear peaks, one at 5 ml/min for the outflux of cells and one at 7 ml/min for the influx of cells.

The amount of movement is dependent on the flow rate of the washing buffer as cells seem to require a certain pushing force to be able to move away from the high gradient region. The peak of cell outflux on the imaged gradient line was lower than the peak of cell influx (Figure 11). As the flow rate required to move cells which are captured more upstream seems to be higher than the flow rate required to move cells on the image line, it might be that there is a stronger retainment of these cells.

Assuming a completely saturated magnetization, equation (14) can be used to calculate the maximum magnetic moment which a cell can have when it is able to move at a certain flow rate. For the imaged line in Figure 10 and Figure 11, the highest amount of outflux happened at 5 ml/min. The peak in influx, which is the highest amount of outflux of the lines upstream, happened at 7 ml/min. Using the equations above with a COMSOL simulated magnetic field (Appendix B), we can find a maximum magnetic moment of $2.2\text{E-}14 \text{ Am}^2$ for cells leaving the imaged line and a maximum magnetic moment of $3.1\text{E-}14 \text{ Am}^2$ for cells leaving the lines upstream. This is the maximum moment of the moving cells because, if the magnetic moment of those cells would have been higher, they would have been retained.

2.3.2.2 Optimizing magnetic setup

The optimal Halbach array outperformed the other two magnets with each tested cell line, as shown in Figure 12. The improvement in recovery is highest for the EpCAM low cell lines PC3 and PC3-9. This makes sense as even without optimization the recovery of LNCaP cells is close to 100%, which leaves not much room for improvement. The sample processed with CellSearch had a 100% recovery of LNCaP cells, a 50% recovery of PC3-9 cells and a 14% recovery of PC3 cells. Thus, each Halbach array showed higher recovery of EpCAM low cells than CellSearch.

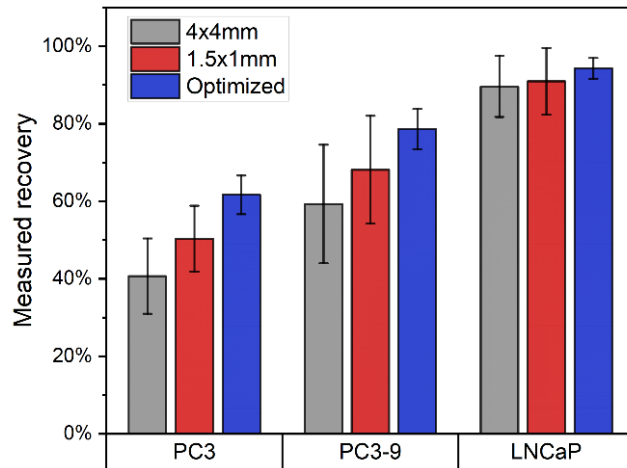


Figure 12: Results of comparing magnets. Graph shows recoveries of the different cell lines per array type.

Using COMSOL simulations, we can use the shift in recovery rates between the different magnet types to calculate the magnetic moment of the used cell lines [21]. For this goal, a distribution in magnetic moment was fitted based on flow cytometry data. Figure 13 shows the distributions in magnetic moments of PC3 and PC3-9 cells, together with the found magnetic moments of PC3-9 cells when imaging in and outflux on a magnetic gradient line. It is visible that both methods find a similar order of magnitude for magnetic moments. Take in mind however that the magnetic moments found earlier are maxima instead of averages or distributions and that a different type of ferrofluid was used.

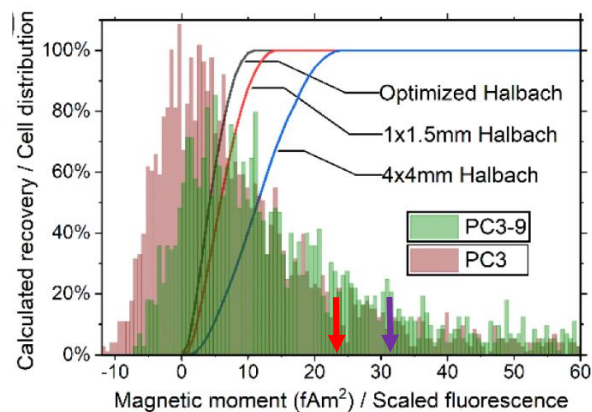


Figure 13: Distribution of magnetic moments based on COMSOL modelling and experimental results for PC3-9 cells and PC3 cells. Arrows show earlier estimations, with red being the imaged line in section [2.3.4.1] and purple cells from the lines upstream.

2.3.2.3 Removing unbound cells

The removal of unbound cells takes place in two steps. Rinsing is the first step, which can be described as flowing additional, clean, buffer through the sample tube and the tubing to ensure all sample has completely passed the system. In Figure 14 it is visible that at least 2 ml of buffer should be used to get a ~90% passing of a 1 ml sample through the system.

For washing, we can see in Figure 15 that the majority of background cells (LCL's) are washed away with the first 2 ml of washing buffer and the effectiveness of washing decreases thereafter. Also, there is little effect of increasing flow velocity on the flushing out of target cells (PC3-9's). After washing with 2-4 ml of washing buffer at 1-2 ml/min, the majority of washable background is depleted.

Sample	Absorption at 413 nm	Concentration	Concentration (cumulative)
Control	1.082	100%	
Waste after initial 1 ml sample flowthrough	0.015	1.39%	1.39%
Waste after rinsing (1 ml)	0.743	68.7%	70.09%
Waste after secondary rinse (1 ml)	0.191	17.74%	87.83%

Figure 14: Results of photo-spectrometry measurements. Concentrations were determined by the percentage of absorption relative to the control sample.

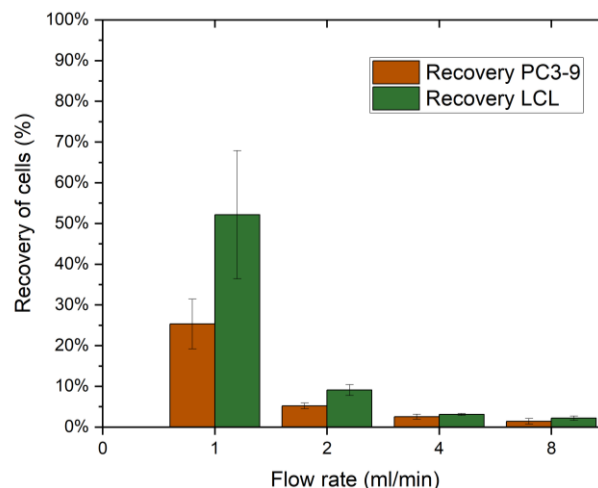
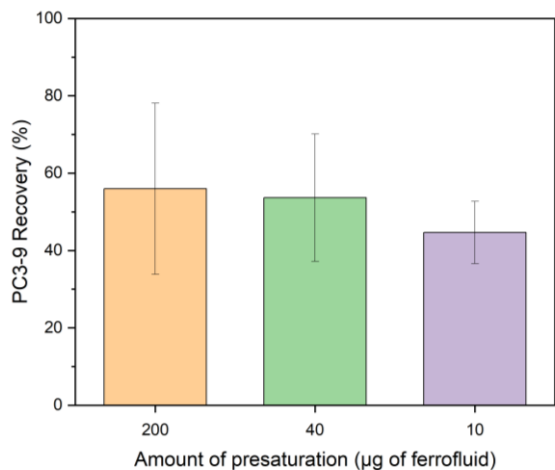


Figure 15: Results of washing experiment. Counts were determined using flow cytometry.

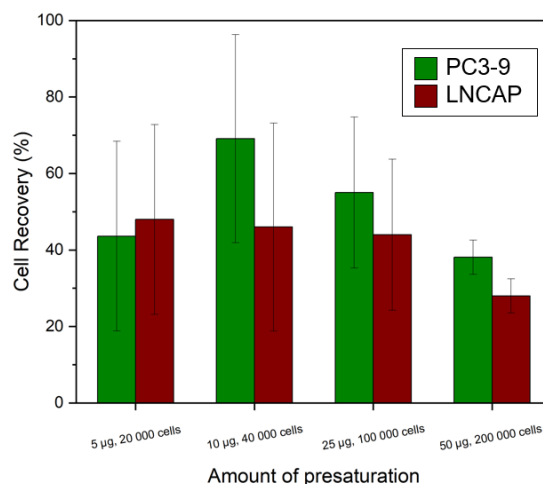
2.3.2.4 Investigating limits in throughput

Pre-saturation of the channel, either with only ferrofluids or cells and ferrofluids, does not lead to a clear trend in terms of decrease or increase in PC3-9 cell recovery, as shown in Figure 16 a,b. Therefore, if there would be any magnetic shielding, the size of it does not seem to increase or decrease with larger amount of ferrofluids. The recovery of PC3-9 cells is lower than in earlier experiments however.

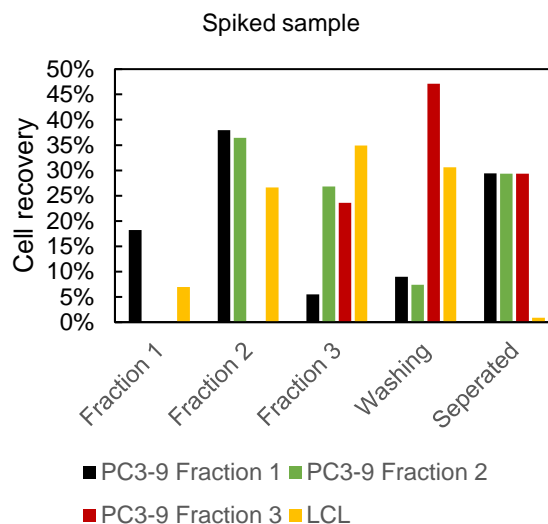
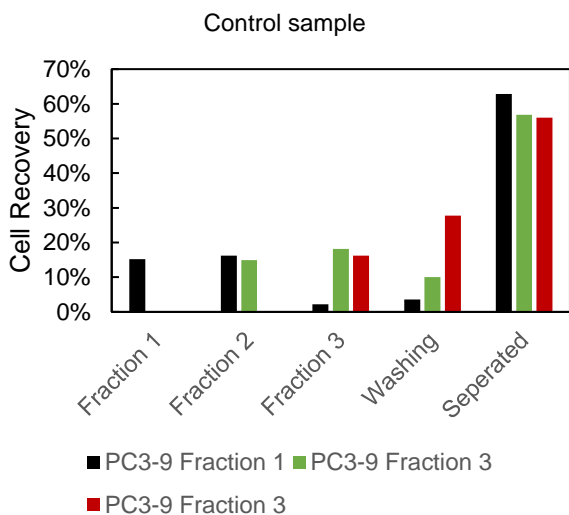
Figure 16 c,d, shows dynamically how cell populations are flushed out during the separation process. It is visible that instead of a continuous outflux of a portion of cells per ml, which would lead to a decrease in recovery for cells which are captured earlier in the process, each population loses a similar amount, which ultimately results into a very comparable recovery for each population. When spiked in a background of millions of cultured leukocytes, the recovery significantly decreases.



a. Recoveries of PC3-9's with channel presaturation using different amounts of streptavidin ferrofluid (Biomagnetic Solutions). Different colors represent different iterations of the experiment.



b. Recoveries of PC3-9 cells with channel presaturation using different amounts of LNCAP's and VU1D9 ferrofluids. The amount of recovered LNCAP cells are also represented. N=3



c. Recoveries of different subsequential fractions of PC3-9 cells which are either separated from 2ml buffer samples or 2 ml samples containing 20E6 LCL cells. N=1

Figure 16: Results of experimentally determining throughput using different methods.

2.3.2.5 Use of parallel processing

The use of three Ibidi chips instead of one allowed us to increase the flow rate threefold while having a similar retention time of cells in the channel, as the surface area is increased with a factor three. For a 10 ml sample this reduced the processing time from 20 minutes using a flow rate of .5 ml/min to 6.6 minutes using a flow rate of 1.5 ml/min. The recoveries in this experiment are shown in Table 2. It is visible that parallel processing has a ~ 17% lower recovery on average in 3 measurements.

Measurement	Recovery 1 chip (# Cells)	Recovery 3 chips (# Cells)	Performance 3 chips (Recovery 3 chips / Recovery 1 chip)
1	12.342	13.642	110.5 %
2	8137	6489	79.7 %
3	9967	5954	59.7 %
Average	10.149	8695	83.3 %

Table 2: Results of comparing parallel processing to the normal situation of 1 chip. Counts determined using flow cytometry.

2.4 Discussion

2.4.1 Optimizing flow conditions

After having used both simulations and experiments, we were able to find optima for flow rate and channel height when performing immunomagnetic enrichment using Ibidi μ -slides. The chip of Hoshino et al. was able to process 10 ml of blood within one hour. We were able to process at higher flow rates but used samples containing only target cells. This is beneficial for accurate measurement and comparability to simulations. Using real samples would lead to non-Newtonian behavior, which is inherently difficult to simulate [19, 27]. Simulations of interactions between tens of millions of cells, each with different properties, will require incredible computing power.

Although we do not simulate real samples, it is safe to say that recovery will be lower when compared to the buffer samples used for optimization of flow configuration and magnetic setup. CTC's will collide on their way to being captured and therefore encounter a larger resistance than simulated. In both situations however, recovery should be as high as possible and broadly speaking the physics and experiments are also applicable to clinical samples.

Furthermore, the model showed a discrepancy with empirical results. While the model was able to calculate cell trajectories in the channel, movement of cells after they were captured was not accounted for. Equation (10) shows that the shear force on captured cells scales with a power 3 to the channel height. This means that for smaller channels the flushing of cells is much higher than with the larger channels, which might explain the optimum which we can find in the experimental results.

The experiment in which the movement of cells between the magnetic gradient lines was imaged during washing did not show any cells actually leaving the channel. Due to the dimensions of the channel, the outlet could not be imaged thus it is merely an assumption that captured cells are able to be flushed out. In further experiments however this ability for captured cells to leave the channel is shown. The experiment did hint to a relation between location in the chip and magnetic moment, with cells of higher magnetic moments being caught more upstream in the chip. This was also expected from the MATLAB model. It would be interesting to image some additional lines upstream and see if a larger flow rate is indeed required to flush these cells.

To conclude, these results further show that it is not only harder to capture cells with few ferrofluids, but it is also harder to retain them in the channel. Therefore, it is important to optimize the magnetic configuration of the magnetophoresis setup, as the equations show that it can benefit both cell capture and retention.

2.4.2 Finding the optimal magnetic array

The experiments of testing multiple magnetic configurations were performed using flow conditions which are considered suboptimal, according to the results of the flow optimization experiments. This was because the starting point should be low enough to be able to see significant results and with optimal flow conditions already a >80% recovery of PC3-9 cells was found. Compared to the situation of separating with a North-South oriented array with 3x12x15 mm N52 magnets, the optimized magnet setup leads to a ~16% increase in recovery. This shows that using the optimized Halbach array is not only the best Halbach array, but also an improvement when compared to the used North-South oriented array.

Additionally, an increase in recovery for PC3 and PC3-9 cells was shown relative to CellSearch. PC3 and PC3-9 cells are relatively low in EpCAM expression. The increase in recovery for EpCAM^{LOW} cells is very relevant, because low recovery rates of EpCAM^{LOW} CTC's is considered a big flaw of CellSearch [28, 29]. To increase magnetic moment of CTC's, CellSearch uses controlled aggregation to create clusters of ferrofluids [30]. This can possibly also applied to a flow-based system to increase CTC recovery.

2.4.3 Removing unbound cells

Effectively removing unbound cells is important for the purity of the output of the system. A system might have a recovery of 100% but if the depletion is 0%, there is no actual work performed at all. One advantage of a flow based system is that there is continuous washing of the captured fraction. With additional washing after separation we can increase depletion but this will also result in a lower recovery. This shows a tradeoff between aggressive washing, with higher depletion and lower recoveries, and gentle washing with opposite effects.

2.4.4 Investigating limits in throughput

When investigating the effects of magnetic shielding, no clear trend could be found. It could be concluded however that even in the extreme amount of 200 μg of iron particles present in the channel, a large portion of PC3-9 cells can be captured.

The experiment in which different batches of cells were processed in sequence shows the capability of captured cells to leave the channel, which was expected after the experiment in which captured cells were imaged while washing. From this we experiment can conclude that the moment in time cells enter the channel is not a relevant determining factor for a successful, retained capture, but their magnetic moment is. Thus, to successfully capture and retain cells, this moment should be as large as possible for CTC's, while it should be as low as possible for leukocytes and erythrocytes.

2.4.5 Use of parallel processing

Parallel processing lead to slightly lower recovery rates while also resulting in a great decrease in processing time. One problem which was encountered is that the total fluid volume of the system is increased when multiple chips are used in parallel. This is not necessarily problematic for the capture of cells but will require larger volumes for rinsing, washing and especially flushing of the chip. The latter is especially problematic as volume reduction of the sample is one of the goals of the device and flushing with larger volumes will lead to a larger volume of the final product.

2.5 Conclusion

In this chapter, factors were determined which influence the recovery of CTC's when enriched using simple microfluidic magnetophoretic systems. For recovery, a flow rate 0.5 ml/min was found to be optimal. Increasing channel height leads to a decrease in magnetic attraction in the upper portions of the channel but a decrease in unwanted outflux of captured cells, which results in an optimum around 600 μm .

For high recoveries, a high magnetic gradient in the channel is very important. A specially built Halbach array of $1 \times 2 \times 15 \text{ mm}^3$ N52 magnets oriented horizontally and $1 \times 2.75 \times 15 \text{ mm}^3$ N52 magnets oriented vertically was found to outperform all other tested configurations.

The sample tube should be properly rinsed before washing to ensure full sample flowthrough. Rinsing with 2 ml of buffer should be considered the minimum. Washing increases depletion of leukocytes which leads to better sample purities. To increase purity, washing should be performed with higher flow rates than separation but this also leads to a loss in recovery. Washing with 2-4 ml of buffer at a flow rate of 1-2 ml/min was found to be adequate.

As for limits in throughput, none have been found thus far. It seems to be the case however that the recovery of a CTC is not dependent on the moment it enters the channel but rather on the total magnetic moment of the cell and bound ferrofluids.

To reduce the processing time the chips can be used in parallel. The use of 3 chips in parallel lead to a 3x reduced sample flow through time but also lead to a 17% reduction in recovery.

3. Fine separation

3.1 Introduction

For downstream CTC analysis techniques, especially genomic assays, single cell CTC's are often required [10, 11, 31]. Single cell isolation platforms have limited processing capacity, ranging from 6000 to 20 000 cells as maximum input [11, 32]. To be able to process a whole DLA sample, this would require a 6 log depletion of leukocytes while CellSearch only reaches a 3-4 log depletion in DLA [16].

Fluorescence Activated Cell Sorting (FACS) is a method to sort cells based on biomarker expression. In a specialized flow cytometry device, a stream of droplets, containing fluorochrome stained single cells is measured by laser. Based on the total fluorescence intensity of these fluorochromes, cells are sorted using voltage deflection plates. The principle of FACS sorting is shown in Figure 17 (left). FACS sorting is a technique which has been used to isolate CTC's before [10].

If we replace the laser – deflection plate system for a permanent magnet, we get a much more simplified version of the cell sorting system which we can use to sort cells based on their magnetic moment (Figure 17, right). Williams et al. (2021, [33]) published a theoretical model of an immunomagnetic sorting device which can sort CTC's in six fractions. Ozkumur et al. (2013, [34]) built a more simple version of such a device which could separate CTC's from leukocytes. Similarly to the design of Williams, Solsona et al. (2018, [35]) produced a sorting device for catalyst particles which could sort into 5 fractions.

All three devices used some sort of flow focusing mechanism to ensure a narrow stream of sample. This is important as each cell should have the same starting position and velocity to have a separation solely based on magnetic moment. Both the Williams and Solsona paper utilize flow confinement to focus the stream of particles in the channel. Ozkumur et al. however used inertial flow focusing to get a narrow stream. Magnetic attraction was done with either a quadrupole magnet setup (Ozkumur), a single bar magnet (Solsona) or a combination of two dipoles (Williams). The production of the chips was done with either reactive ion etching (Ozkumur) or SLS 3D printing (Solsona). Table 3 shows a short overview of the three chips.

In this chapter, the goal is to separate cells into three fractions; 'EpCAM High' CTC's, 'EpCAM Low' CTC's and 'EpCAM negative' waste. Altering magnetic attraction and flow rates can shift distribution of cells over these populations and therefore allows for filtering cells based on their magnetic moment and therefore EpCAM expression.

Such a magnetic sorting setup can also be used to perform measurements on the cells themselves. As the amount of attraction is related to the magnetic moment of the cells, the trajectories of the cells can be related to the their magnetic properties. This requires imaging of cells streaming in a known magnetic field. The technique is called particle image velocimetry and can be performed using basic particle tracking techniques [36, 37].

	Williams	Ozkumur	Solsona
Goal	CTC characterization	CTC enrichment	Catalyst particle sorting
Flow focusing	Flow confinement	Inertial focusing	Flow confinement (3D)
Fractions	6	2	5
Magnetic attraction	2 Dipole magnets	Quadrupole magnet	Single bar magnet
Production	-	Reactive ion etching	SLS 3D Printing

Table 3: A short summary on the three devices which inspired the sorting chip. The Williams system is merely a model and the design is therefore hypothetical.

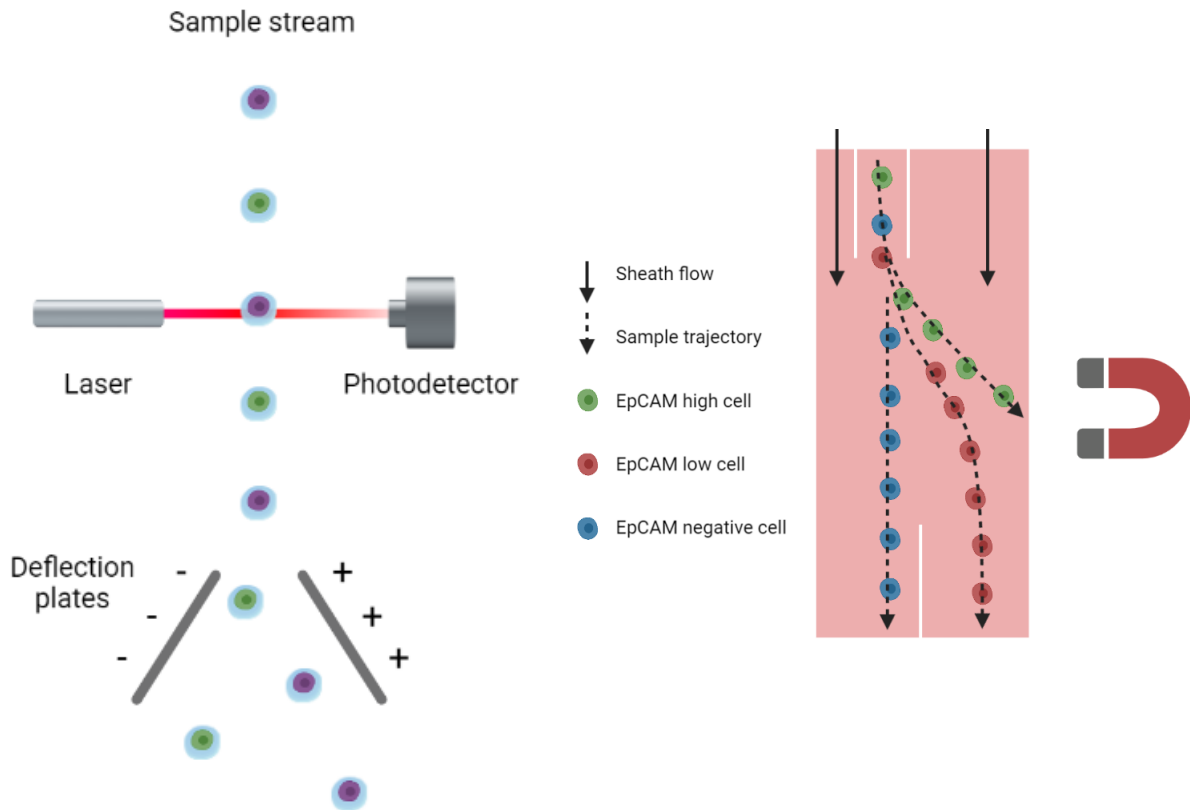


Figure 17: Left: A schematic overview of Fluorescence Activated Cell Sorting (FACS). Cells are suspended in charged droplets, scanned with a laser and deflected by deflection plates. Right: The principle of the magnetic sorting chip. Cells enter the channel in a narrow stream and get attracted by the magnet. The amount of attraction is dependent on the amount of particles on the cell.

3.2 Method

3.2.1 COMSOL modelling

The separation chip was modelled using COMSOL Multiphysics 5.3. The flow field was calculated using the 'Laminar Flow'-interface of the Computational Fluid Dynamics module. The magnetic field and gradients were calculated using the 'Magnetic Fields, No Currents'-interface of the AC/DC module. Particle trajectories were calculated using the 'Particle Tracing for Fluid Flow'-interface of the Particle Tracing module.

Each simulation was performed in two steps. First, a stationary simulation was performed in which the flow field was calculated. The flow rate was set to mass flow, with a defined water mass flowing in each inlet and all outlets set to prevent back flow. Simultaneously, the magnetic field and magnetic field gradient were calculated. The magnets were assumed to be N52 magnets and simulated to have a unidirectional permanent magnetization of 1160 kA/m, perpendicular to the flow. The liquid in the chip and the air surrounding the chip were set to have a relative magnetic permeability of 1.

Then, a time dependent simulation was performed. The particle distribution and initial flow velocities were set to match the flow profile. The relative magnetic permeability of the particles were defined using equations (9) and (10) from chapter 2. The simulation was run each time for 500 seconds and particles were considered caught when they touch the channel wall.

3.2.2 Chip production

3.2.2.1 Iteration one

Design Choices

The channel dimensions (width and length) were roughly based on the Ibidi chips used in the experiments for rough separation. As these are known to work for similar purposes, it is a logical starting point. Like the Ibidi chip, 4mm wide Leur inlets were used to connect the chip to tubing and pump. To get the magnets as close to the channel as possible, a notch was made. A small channel depth of 100 μm should ensure that cells have roughly the same velocity. A small inlet channel width of 200 μm should focus the cells in the stream.

Production

A 0.1x5x50 (DxWxL) mm separation channel was milled into a piece of translucent PMMA, together with a 200 μm wide sample inlet, a sheath flow inlet and two outlets (Figure 18). Top and bottom plates were bonded using two sided adhesive tape. All inlets are 4 mm wide and Leur connectors were glued onto top plate with two component epoxy. A 5 mm deep notch for the magnet was made using a bandsaw. Due to production error, a small extra hole was produced in the inlet (Figure 19).

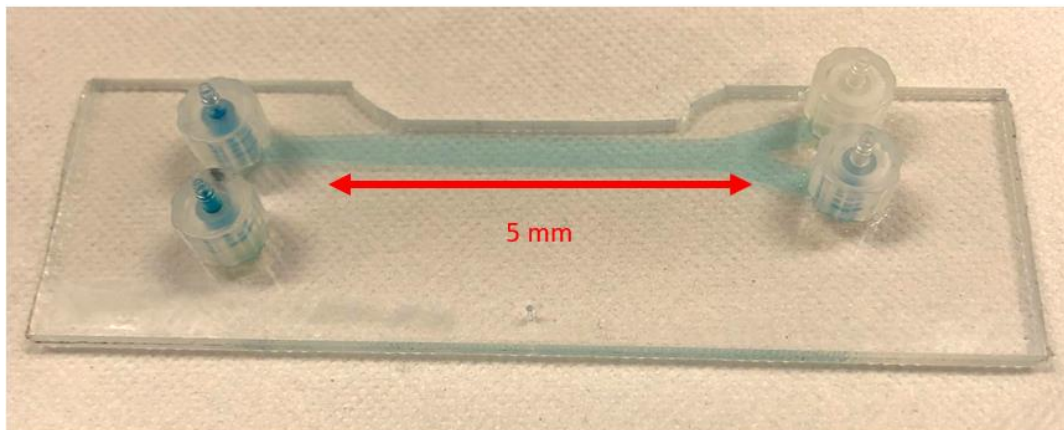


Figure 18: Photograph of chip version 1. Channel was filled with food coloring dye for visualization.

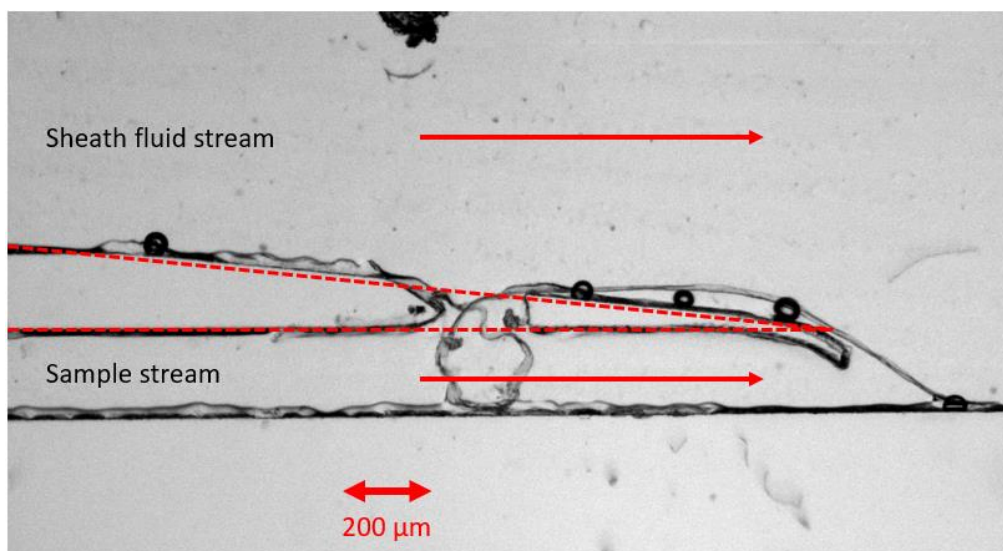


Figure 19: Microscopic image of sample inlet (10x objective). Red dotted line shows how the inlet was intended to look.

3.2.2.2 Iteration two

Design Choices

To increase the average magnetic attraction forces in the channel, the channel width was decreased to 2.5 mm. To alleviate bubble formation problems, the channel depth was increased to 400 μm , which should make possible bubbles more mobile and their presence less problematic. As the Luer sample inlet of 4mm created a problem of cell sedimentation, a new sample inlet design was made, consisting of a 200 μl Eppendorf tube which acts as reservoir (Figure 20).

Production

A 0.4x2.5x50 (DxWxL) mm separation channel was milled into a piece of translucent PMMA, together with a 200 μm wide sample inlet, a sheath flow inlet and two outlets (Figure 21). This iteration, also the 4mm deep notch for the magnet, which was previously sawed out, was milled. Top and bottom plates were bonded using two sided adhesive tape. 4 mm Luer connectors were used for sheath flow inlet and sample outlets, the sample inlet was connected via the Eppendorf tube. This way, the reservoir is easily accessible at all times. All connectors were glued on using two component epoxy.

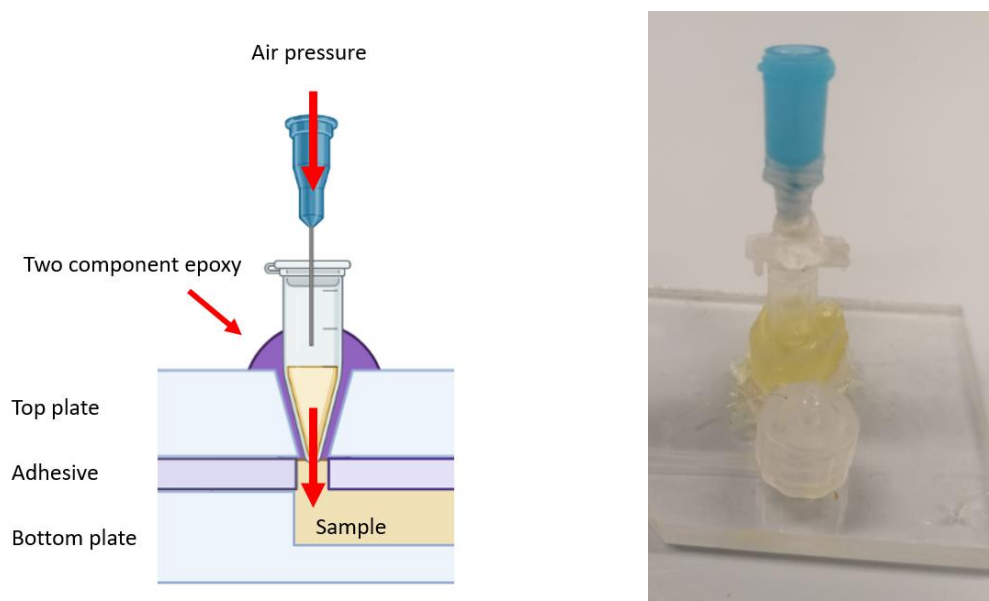


Figure 20: Left: schematic depiction of how the reservoir is connected to the chip. Right: Photograph of the actual chip, visible is the glued on Eppendorf tube and the Luer-connector.

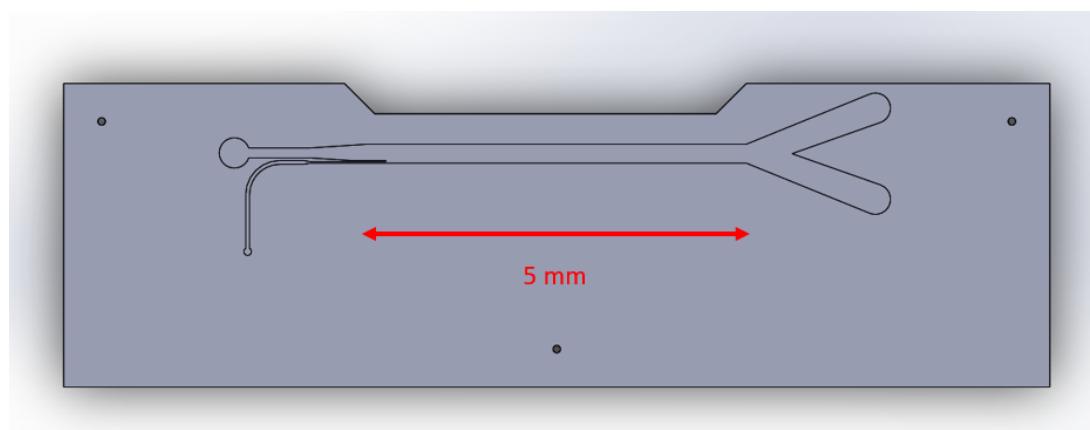


Figure 21: Solidworks model of the design, showing inlets on the left and outlets on the right. Upper left inlet is sheath flow inlet, lower left inlet is sample inlet.

3.2.2.3 Iteration three

Design Choices

The channel dimensions used in iteration 2 were deemed adequate, and the main alteration in design was creating an additional sheath flow channel alongside the sample channel. A problem encountered with iteration 2 was that unattracted cells were pushed to the channel wall. The extra sheath flow channel was created to prevent this. The dimension of this channel were similar to that of the sample inlet. The split in the outlet channel of iteration 2 created a dead-flow zone where cells were collected. This was fixed by changing the size of this region as shown in Figure 22.

Production

A 0.4x2.5x50 (DxWxL) mm separation channel was milled into a piece of translucent PMMA, together with a 200 μm wide sample inlet, two sheath flow inlets (one small one large) and two outlets (Figure 23). The sample inlet was built in a similar way as shown in Figure 20. Again, top and bottom plates were bonded using two sided adhesive tape and 4 mm Luer connectors were used for the two sheath flow inlets and sample outlets.

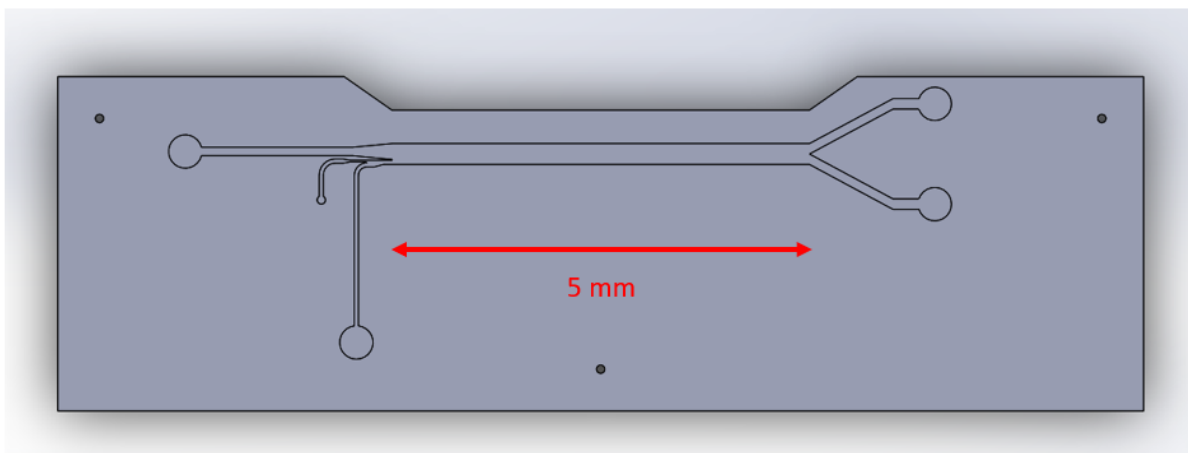


Figure 22: Solidworks model of chip design iteration 3, showing inlets on the left and outlets on the right. Middle left inlet is sample inlet, outer left inlets are sheath flow inlets.

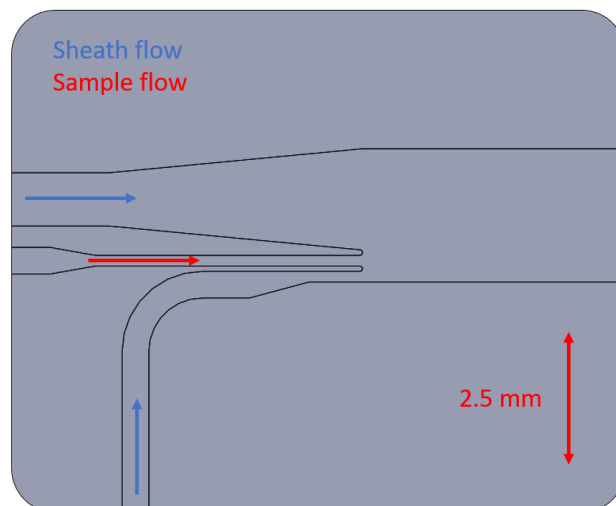


Figure 23: New design of sample inlet. Blue arrows labels sheath flow inlets, red arrow labels sample flow.

3.2.3 Experimental testing

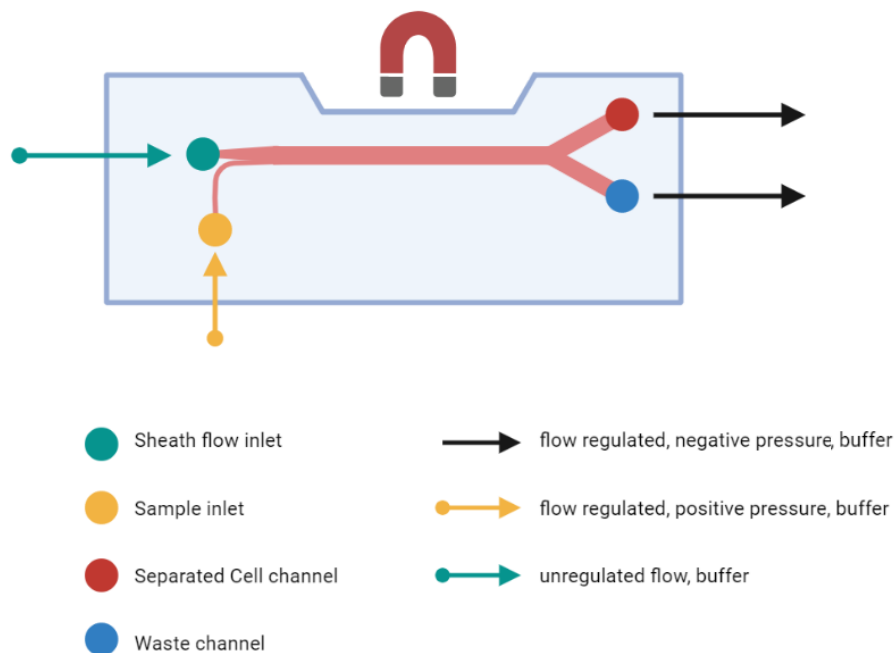
3.2.3.1 Operation of the sorting device

As there are multiple inlets and outlets to control, operation of the sorting chip is not as straightforward as operating the Ibidi chip. In the sorting device cells are attracted over relatively large distances, therefore the flow rate was set quite low in order to ensure enough retention time in the chip. Sheath flow rates in the range of 10-50 $\mu\text{l}/\text{min}$ were used. When using the first chip iteration (Figure 24 a), the sample was injected using a syringe pump containing a 1 ml syringe. As the sample rate is much lower than the sheath flow rate, the sample had to be highly concentrated to reach a workable cell throughput.

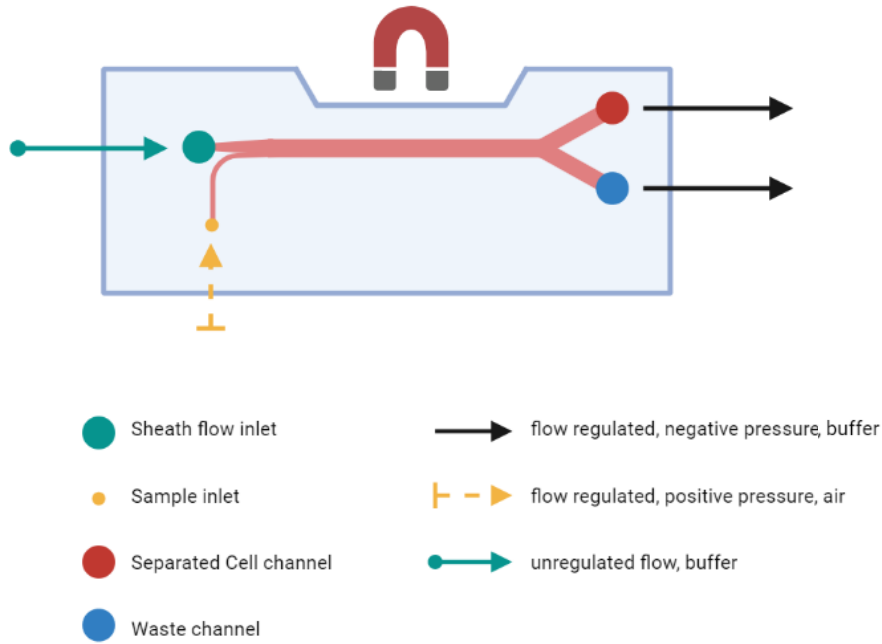
Switching the sample inlet to an Eppendorf based reservoir made loading the sample much easier with chip V2 (Figure 24 b). This design required a pressure buildup in the sample reservoir, which was done using a syringe pump that pumped air into the reservoir. The sample flow rate was considered to be similar to that of the air which was pumped in.

In chip V3 (Figure 24 c), an additional sheath flow inlet was placed. This additional sheath flow stream was injected from a syringe pump with the same flow rate as the sample.

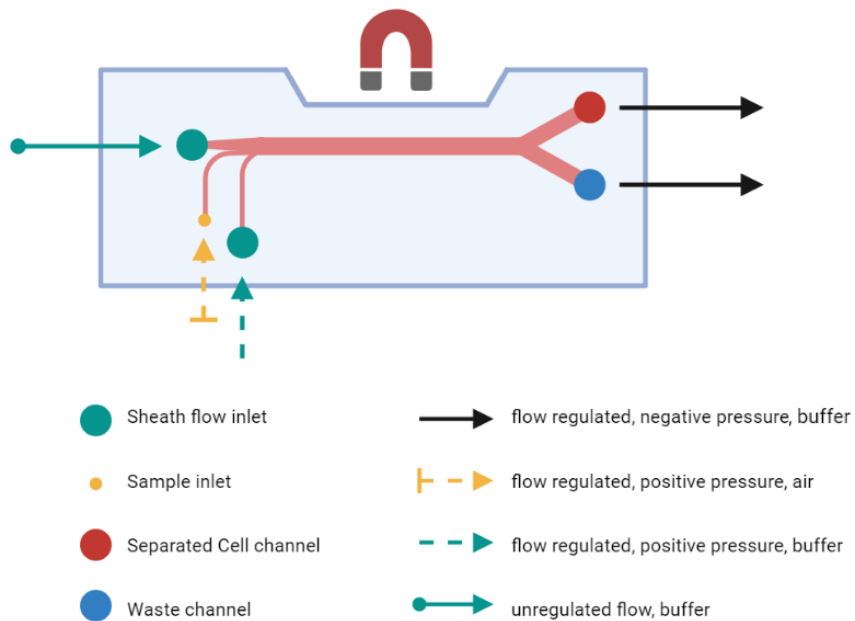
To prevent cells from flowing back into the sheath flow inlet, it is important to create an overpressure between the sheath flow inlet and the sample channel. This is achieved by placing the sheath flow buffer reservoir above the chip, creating hydrostatic pressure. When using air pressure to drive the sample flow, the hydrostatic pressure should be kept low enough however in order to prevent sample from being pushed back into the sample inlet.



a. Flow regulations of chip 1. Sample channel was regulated with positive pressure, pushing the sample in the channel. Outlets are controlled with negative pressure, pulling the liquid through both channels equally.



b. Flow regulations of chip 2. Sample channel was regulated with positive pressure, applied as air on the Eppendorf based on chip sample reservoir, pushing the sample in the channel. Outlets are controlled with negative pressure, pulling the liquid through both channels equally.



c. Flow regulations of chip 3. Sample channel was regulated with positive pressure, applied as air on the Eppendorf based on chip sample reservoir, pushing the sample in the channel. One of the sheath flow inlets was unregulated, the other was regulated with positive pressure, set to the same flow rate as the sample channel. Outlets are controlled with negative pressure, pulling the liquid through both channels equally.

Figure 24: Graphic depiction of flow regulations used in different iterations of the sorting device. a-c represents iteration 1-3.

3.2.3.2 Flow focusing

As the goal of the chip is to sort cells based on magnetic moment, a narrow stream of cells was required such that all cells encounter a similar magnetic field. A series of experiments was performed to investigate two factors which are important for flow focusing; velocity distribution and spatial distribution. Velocity distribution is closely related to the spatial distribution over the channel height, as cells roughly travel with the velocity of the buffer. Furthermore, the starting distance between the cells and the magnet should be similar for each cell, thus the spatial distribution over the channel surface should also be similar.

Gravitational focusing

COMSOL Modelling

A simplified 3D version of the SOLIDWORKS model used to produce the chip was used to calculate 3D flow profiles of the fluids in the chip in COMSOL (Figure 25). Using the calculated profile, it was possible to determine the position of cells in the channel by measuring their velocity and 2D position.

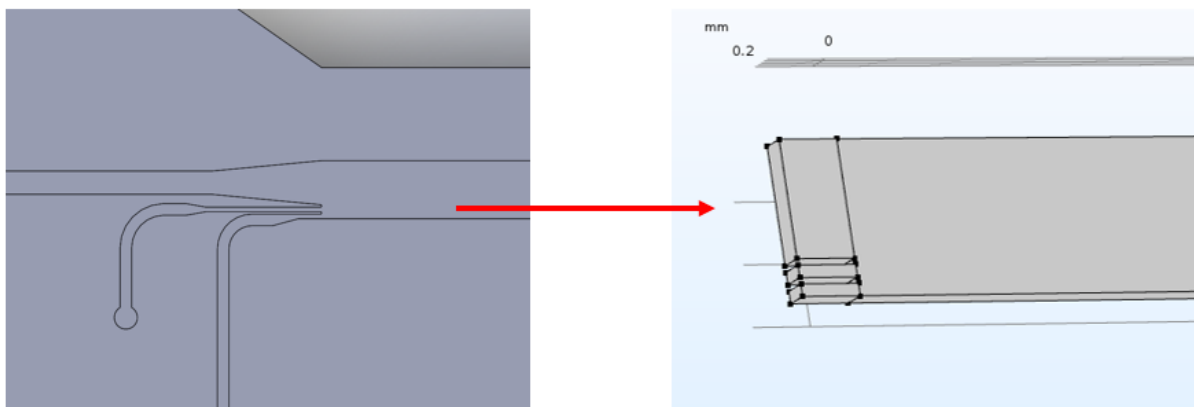


Figure 25: A visual representation of the simplifications which were made in the COMSOL model. Inlet and channel dimensions are kept consistent.

Measuring flow velocities

To visualize the locations of cells in the channel, LNCAP cells were incubated with CellTracker Orange (CTO) for 30 min at room temperature and washed. Then the cells were flown through the chip using flow rate of 20 $\mu\text{l}/\text{min}$ at both outlets, and 2 $\mu\text{l}/\text{min}$ at the sample inlet and additional sheath flow inlet. The cells were filmed with a microscope while flowing through the channel. This was done for both the situation with the microscope and chip in horizontal position (flow perpendicular to gravity) and vertical position (flow parallel to gravity).

The framerate of the video was determined to be 4.93 FPS. Using a specialized calibration tool, we could determine the FOV of the video frame in horizontal direction (which is the axis the cells are flowing along) to be 1050 μm . Using manual analysis, it was possible to count the amount of frames that a cell was in view, and using the FPS and FOV we could then calculate how fast a cell was flowing.

Spatial focusing

The width of the sample stream in the chip could be measured with microscopy. Cells were incubated with CellTracker Orange and flushed through chip 2 and chip 3 at different rates of sample- and sheath flow. During flow, cells were imaged and videos were produced. These videos were manually analyzed to determine the width of the sample stream.

The following combinations were tested:

Chip	Sample Flow rate	Sheath Flow Rate	Ratio
Chip 2	2 $\mu\text{l}/\text{min}$	40 $\mu\text{l}/\text{min}$	1:20
Chip 3	2 $\mu\text{l}/\text{min}$	40 $\mu\text{l}/\text{min}$	1:20
Chip 3	5 $\mu\text{l}/\text{min}$	20 $\mu\text{l}/\text{min}$	1:4
Chip 3	10 $\mu\text{l}/\text{min}$	10 $\mu\text{l}/\text{min}$	1:1

Table 4: Combinations of chips, and flow ratios for sample flow and sheath flow which were used for testing.

3.2.3.3 Magnetic configuration

Unlike the rough separation chip, where the magnetic attraction should be as high as possible, there is much more nuance in creating a magnetic configuration for sorting. You want to divide cells over different fractions rather than just capturing them all in one place.

To see how the use of different magnetic fields influence the distribution of cells over the different fractions, the COMSOL model was configured to test three configurations consisting of either one, two and three $10 \times 10 \times 35 \text{ mm}^3$ N52 magnets. This was compared to an experimental setup. In both cases, three populations of cells were tested:

- For the EpCAM high cells, which were modelled to have a maximum magnetic moment of one pAm^2 , LNCAP cells were used.
- For EpCAM low cells, which were modelled to have a maximum magnetic moment of 0.2 pAm^2 , PC3-9 cells were used.
- For the EpCAM negative cells, which were modelled to have a maximum magnetic moment of 10 fAm^2 , LCL cells were used.

For the experiment, cells were first stained with different CellTracker dyes. Then, 100 000 LNCAPS, 100 000 PC3-9 cells and 20 million LCL cells were spiked in 10 ml of PBS. These cells were incubated for 3×10 min in a quadrupole magnet with 3.3 $\mu\text{g}/\text{ml}$ of CellSearch ferrofluids. After the first 10 min of incubation, 150 μl of capture enhancement reagent was added. After the primary incubation, a 20 min separation was performed. The cells were suspended in a much smaller volume of 500 μl and a secondary incubation, thus with a much higher ferrofluid concentration, was performed overnight.

For both the experiment and the model, the sample rate was set to 2 $\mu\text{l}/\text{min}$ with a 40 $\mu\text{l}/\text{min}$ sheath buffer rate. The trajectories of the cells in the experimental model were imaged using fluorescence microscopy at different points of interest.

3.2.3.4. Cell sorting based on magnetic moment

As the magnetic moment of the cells determine in which population these end up, the amount of ferrofluids on the cells should differ from population to population. To investigate whether this is true, LNCAP cells were first stained with 1 $\mu\text{g}/\text{ml}$ of CellSearch ferrofluids for 3x10 min in a BD magnet array. Then, using centrifugation (500g, 5 min) and aspiration, the unbound ferrofluids are washed away. The ferrofluids are then stained with 5 $\mu\text{g}/\text{ml}$ goat anti-mouse IgG PE (Thermo Fisher Scientific, catalog # A10543) for 30 min at 37°C. Cells were washed and then flushed through chip V2, with 2 magnets attached. A sample : sheath flow ratio of 2 : 40 $\mu\text{l}/\text{min}$ was used. During flow, the separated and waste fractions were collected. After 1 hour of flowing, the sample stream was stopped and the chip was washed for another 30 min with 40 $\mu\text{l}/\text{min}$ of sheath buffer. The magnet was then removed and the caught fraction was captured. The samples were then analyzed with flow cytometry for PE expression.

3.2.3.5. Particle image velocimetry for measuring magnetic moment

As we can use the chip to deflect cells into populations with different magnetic properties, we can also use the chip to calculate the magnetic properties of different cells. If we image cells flowing through the chip, we can measure their velocity towards the magnet and use the physics we already know to estimate the magnetic moment of the cells. This can be used for example to evaluate the quality of different types of magnetic beads for immunomagnetic enrichment.

For this experiment, 3 types of ferrofluids were evaluated: anti-EpCAM CellSearch ferrofluid, anti-EpCAM ferrofluid from Biomagnetic Solutions (BS) and in house produced ferrofluids labeled with streptavidin. LNCAP cells were used, which were stained with CellTracker Orange. The CellSearch and BS ferrofluids were incubated at 10 $\mu\text{g}/\text{ml}$ for 3x10 minutes at a magnet array. For the in house ferrofluids, cells were first labeled with VU1D9 biotin at a concentration of 5 $\mu\text{g}/\text{ml}$ for 30 min at 37 °C, washed and then labeled with 10 $\mu\text{g}/\text{ml}$ of the ferrofluids for 30 min on a roller bank. Around 600 000 cells were labeled per ferrofluid type.

A similar experiment was performed on LNCAP cells which were first stained with anti-EpCAM BV605 HO3 antibodies. These cells were sorted using FACS sorting into two populations, one with high EpCAM expression and one low. After sorting these cells were incubated with CellSearch ferrofluids and CellTracker Orange and velocimetry was performed.

Trajectories were imaged using a Nikon T400 Eclipse microscope. A 4x objective was used and movies were made using a framerate of 399 frames per min. These movies were saved as .avi files which were loaded into MATLAB. Within MATLAB, a specially designed algorithm was applied to process the movies and calculate magnetic moments of the cells in the movie³. This algorithm is shown schematically in Figure 26. First, all frames were segmented with a segmentation filter. Then, blob detection was performed using the MATLAB function *bwconncomp*. This function detects connected components of all shapes and sizes and saves their location, area and shape (centroids).

These features were then used in the particle tracking algorithm, which tracks similar cells in the video. The found trajectories were filtered and only trajectories containing more than five frames were saved. The velocity towards the magnet (perpendicular to the stream) was then calculated using the framerate and the scale of the video, which were both known. Using equation 8 (page 10) together with the modelled magnetic field and field gradient, we could use this to calculate the magnetic moments of the cells.

³ The complete software is available for download on GitHub, through: <https://github.com/TomNiessink/CellTracker>

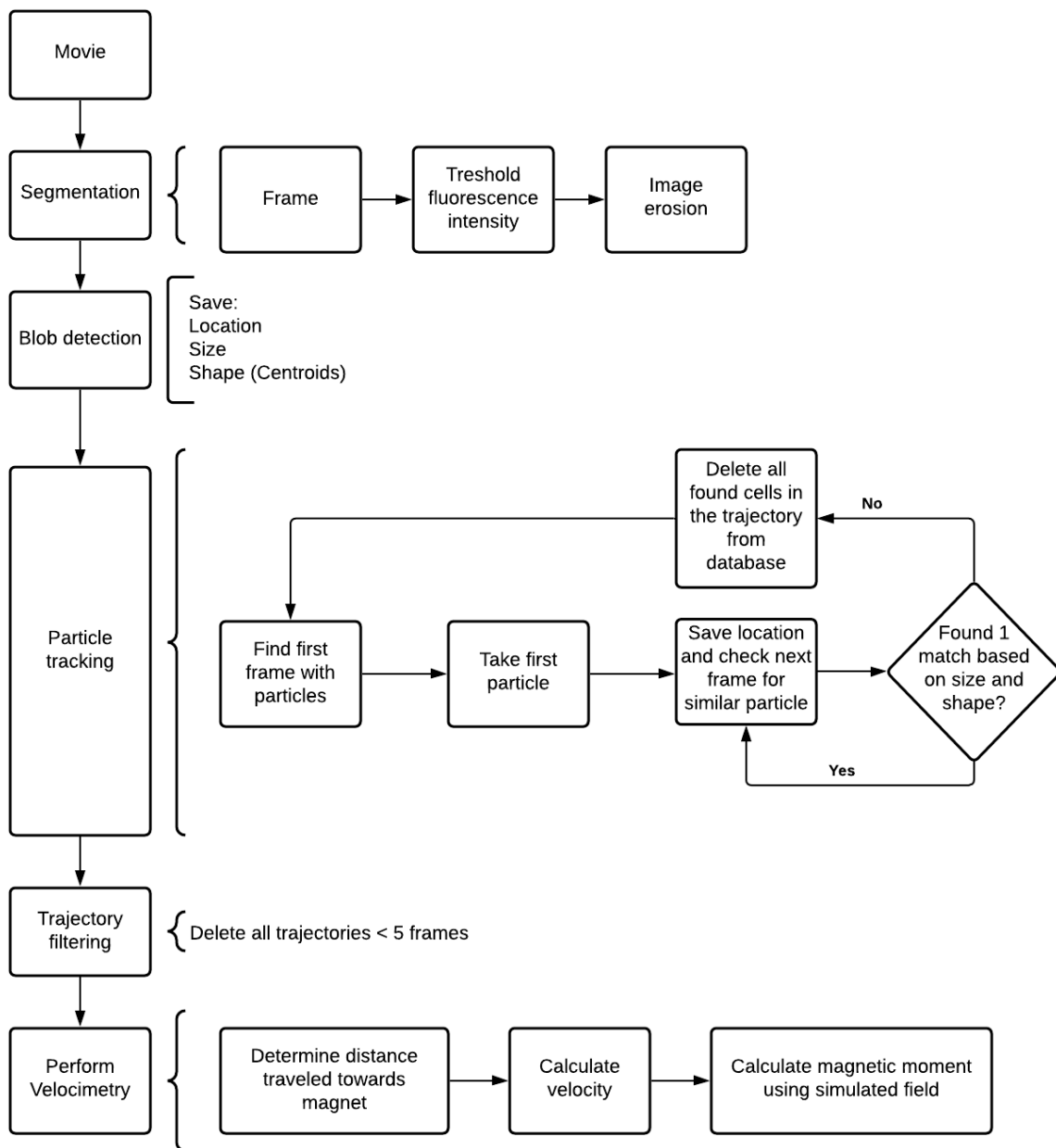


Figure 26: A schematic overview of the particle image velocimetry algorithm for determining magnetic moments of cells.

3.3 Results

3.3.1 Flow focusing

Gravitational focusing

The influence of gravity on cell velocities was examined using the built model and experiments. Figure 27 shows the results of modelling flow profiles in the channel using COMSOL. The parabolic flow profile which is typical for laminar flows is visible. Figure 28 shows the results of measuring the flow velocities of cells with flow oriented either perpendicular (Chip Horizontal) or parallel (Chip Vertical) to gravity.

If we regard the results of the measurement and look in the simulated flow profiles where the cells are flowing in the channel, it is clearly visible that the cells in the horizontal orientation, with gravity perpendicular to flow direction, are all in the bottom of the channel, while the cells in the vertical chip orientation, with gravity parallel to flow direction, are spread out over the height of the channel (Figure 25). The direction of gravity did not influence the spatial spread over the width of the channel.

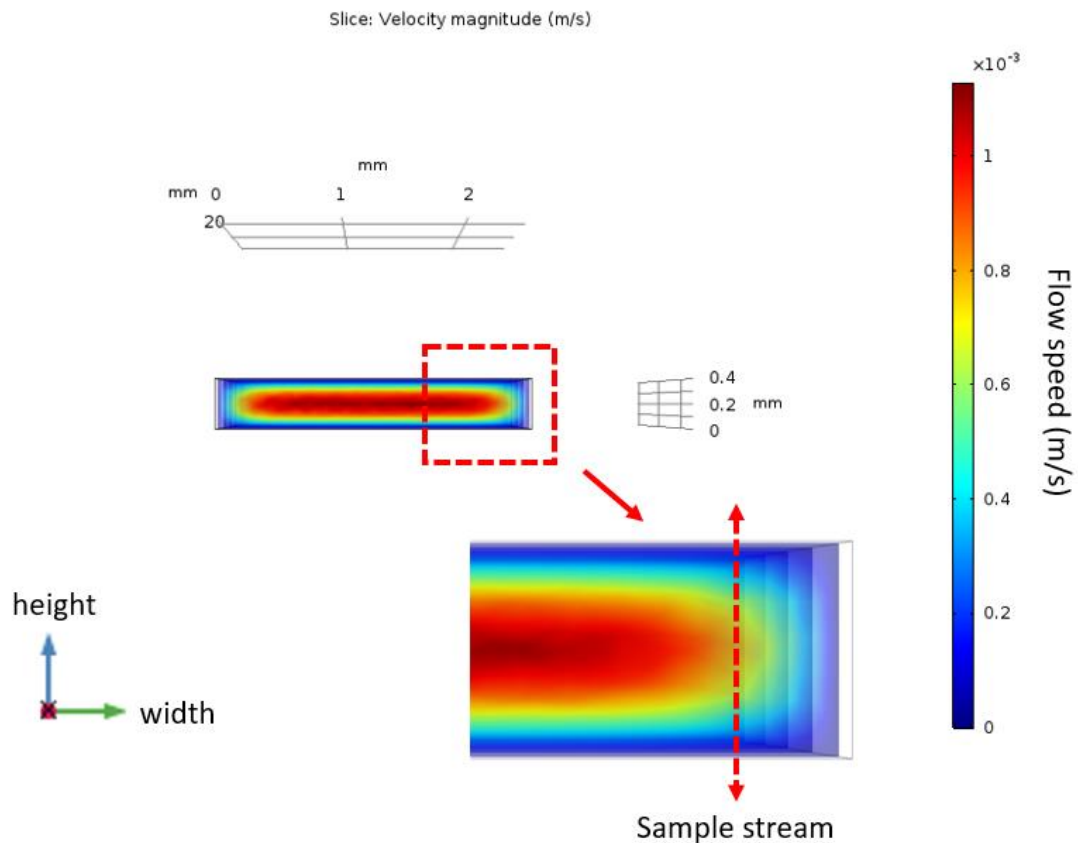
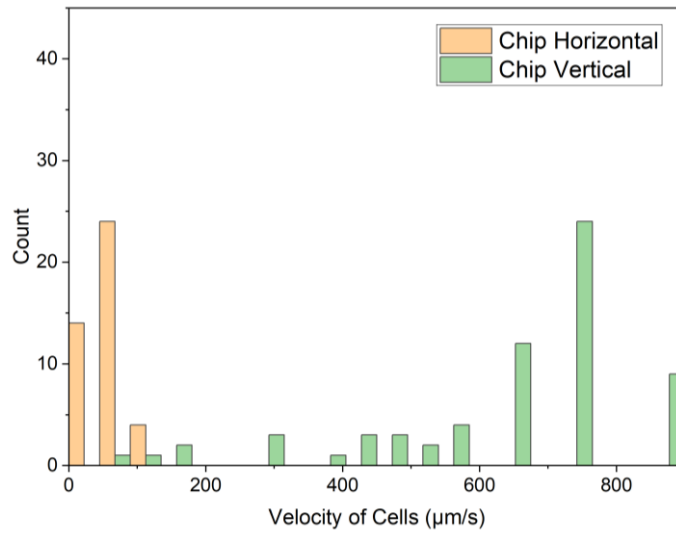


Figure 27: Results of modelling the flow through the flow chip. The dotted red line shows the area which was imaged during flow, which is the sample stream.



<i>Chip Horizontal</i>		<i>Chip Vertical</i>	
Average	53 µm/s	Average	633 µm/s
Standard deviation	18	Standard deviation	193
CV	34%	CV	31%

Figure 28: Results of measuring and calculating the flow velocities in different orientations. Chip Horizontal is the orientation with flow perpendicular to gravity, Chip Vertical is the orientation with flow parallel to gravity.

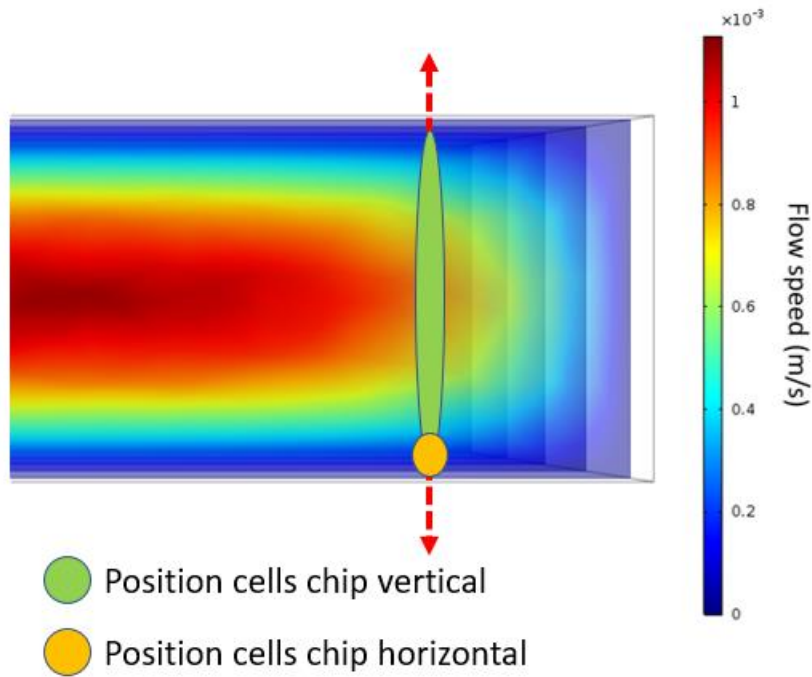
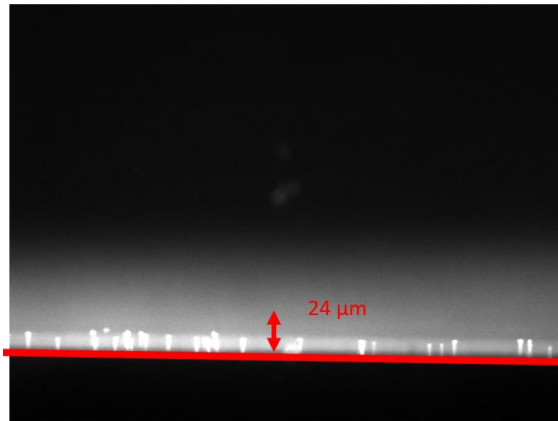


Figure 29: A rough depiction of where the cells are in the channel in both orientations. The red arrow depicts the sample stream. Chip vertical represents the situation with flow parallel to gravity, Chip horizontal represents the situation with flow perpendicular to gravity.

Spatial focusing

To investigate the spatial focusing of cells in the sorting channel, an additional sheath flow inlet was inserted in iteration 3 to better suspend cells in the channel. Figure 30a shows that in chip version 2, without the additional sheath flow inlet, cells are touching the channel wall. Figure 30b shows that the extra inlet indeed helps in creating a suspended cell stream. The spatial focusing however drops significantly, thus this is a tradeoff.

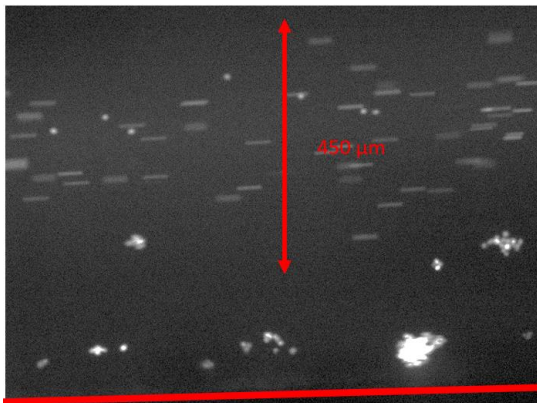
Of the three sample to sheath flow ratio's tested with chip V3, (respectively 1:1, 0.25:1 and 0.05:1) 0.05:1 worked best. This was performed with a sample ratio of 2 $\mu\text{l}/\text{min}$ and a sheath flow ratio of 40 $\mu\text{l}/\text{min}$.



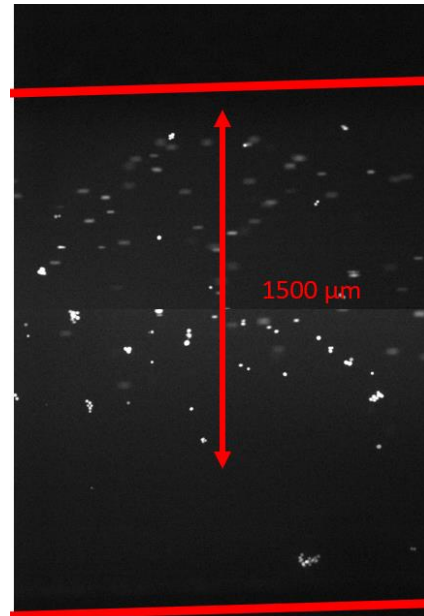
a. Chip 2, sample flow rate 2 $\mu\text{l}/\text{min}$, sheath flow rate 40 $\mu\text{l}/\text{min}$.



b. Chip 3, sample flow rate 2 $\mu\text{l}/\text{min}$, sheath flow rate 40 $\mu\text{l}/\text{min}$.



b. Chip 3, sample flow rate 5 $\mu\text{l}/\text{min}$, sheath flow rate 20 $\mu\text{l}/\text{min}$.



b. Chip 3, sample flow rate 10 $\mu\text{l}/\text{min}$, sheath flow rate 10 $\mu\text{l}/\text{min}$. Image shows two frames, such that the whole channel is visible.

Figure 30: Stills from videos made with fluorescence microscopy. Red lines represent channel walls. Arrows represent the measured width.

3.3.2. Magnetic configuration

Using COMSOL modelling and experiments, we can clearly see how different magnetic configurations (1, 2 or 3 magnets placed in a row) influence the trajectory of cells in the channel. With one magnet, as shown in Figure 31, we are already able to separate the EpCAM high fraction from the other two fractions. The EpCAM high fraction shows a very high attraction to the magnet and gets caught easily. This is shown both in the COMSOL model as with experiments. We can also see that in the beginning of the channel, cells are flowing in the same group. Later on, we can indeed separate EpCAM low cells from EpCAM negative cells, but not with the same accuracy as the model predicts, as there are quite some PC3-9 cells found in the same channel as LCL's.

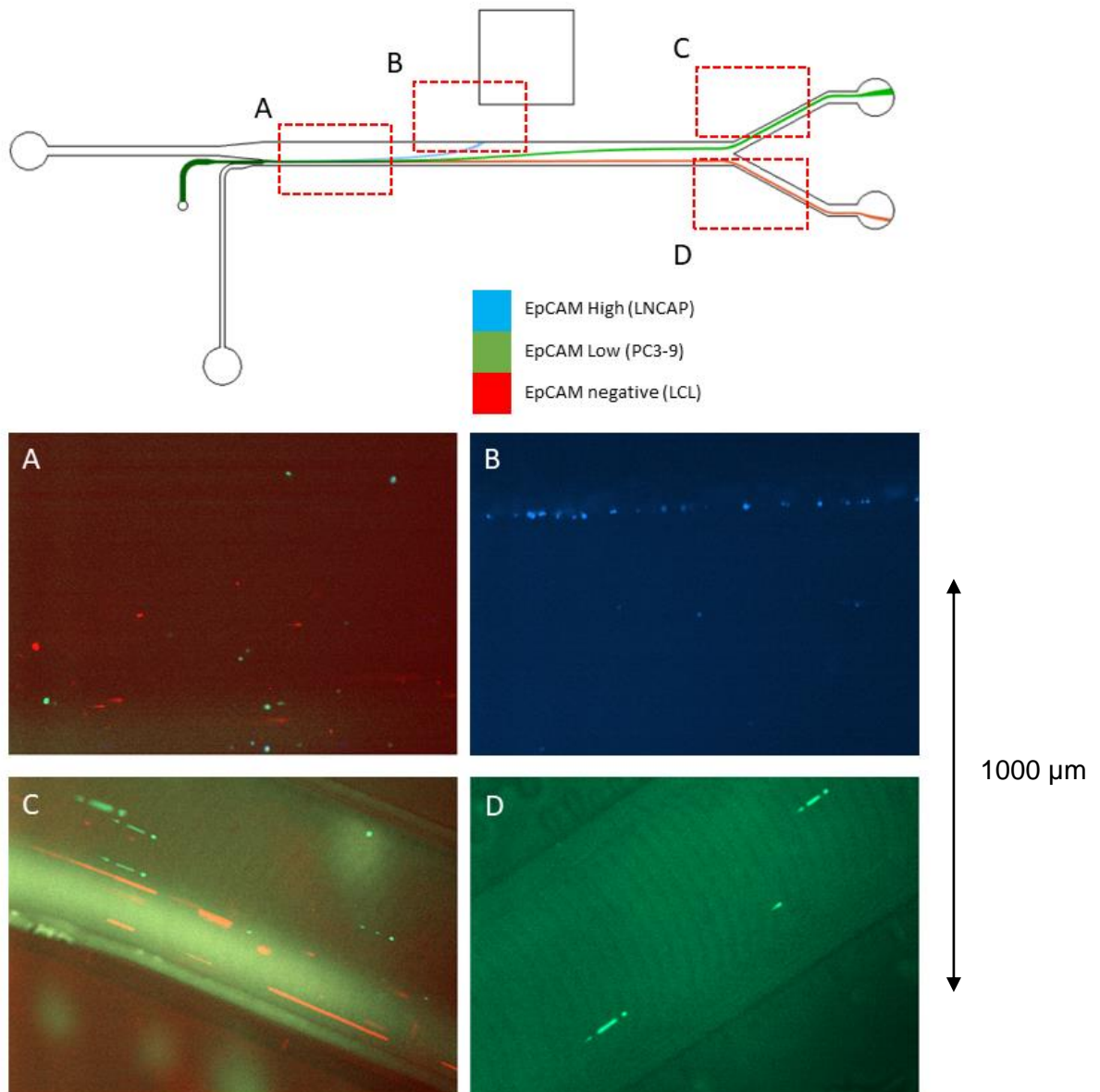


Figure 31: Results of calculating and imaging trajectories of EpCAM high, EpCAM low and EpCAM negative cells in the sorting channel with one magnet. The trajectories in the chip are calculated with COMSOL, images are made with fluorescence microscopy. Colors of trajectories match with colors of cells.

For two magnets, LNCAP's are captured in the same place as before, as visible in Figure 32a. In the middle of the channel, it is visible in Figure 32b how some of the PC3-9 cells are attracted and move away from the sample stream, while others don't. PC3-9 cells are now not only found in the separation channel, but are also being caught in the chip, close to the channel outlet which is on the magnet side (Figure 32c). The waste outlet with LCL cells shows less presence of PC3-9 cells (Figure 32d).

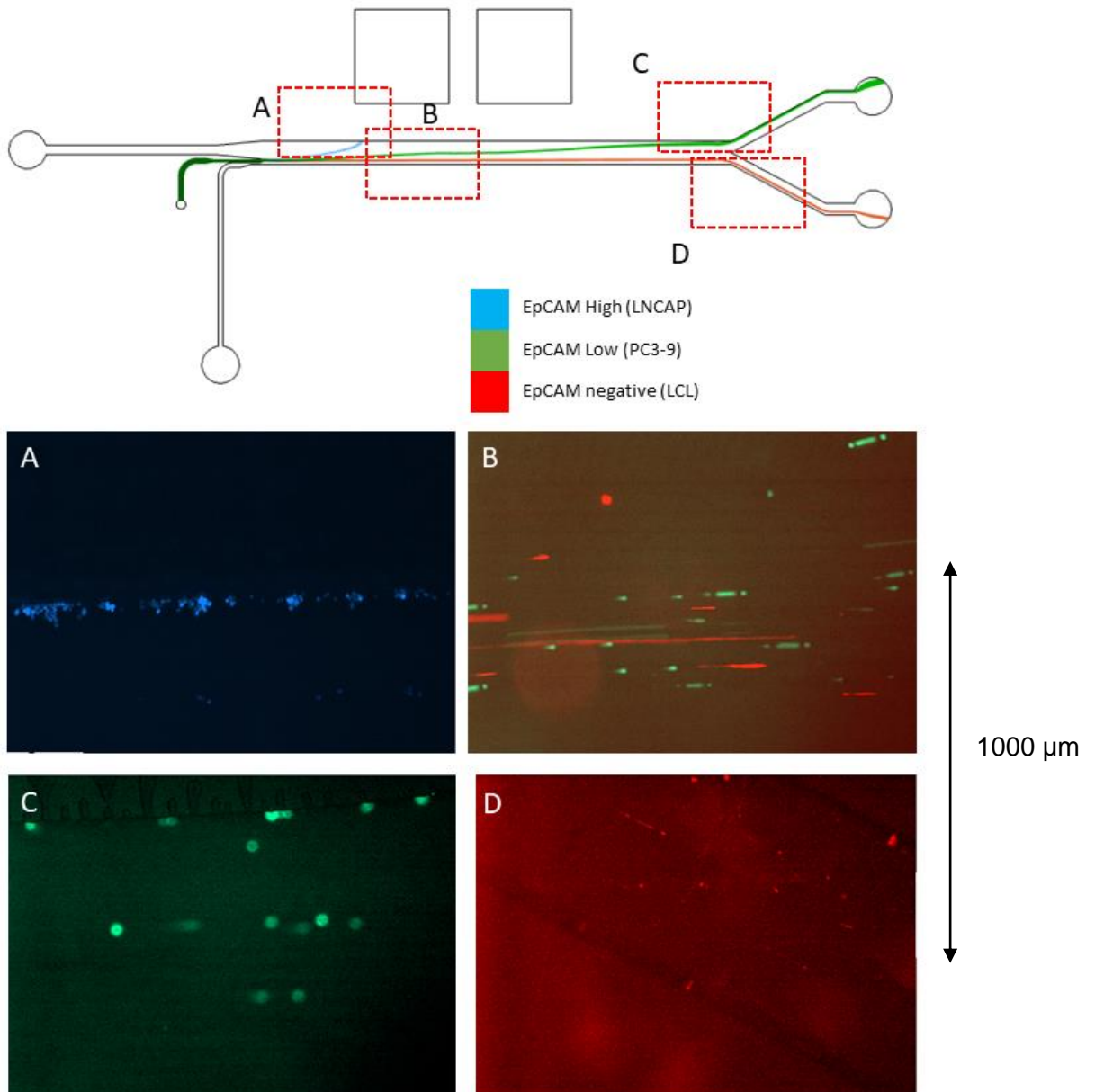


Figure 32: Results of calculating and imaging trajectories of EpCAM high, EpCAM low and EpCAM negative cells in the sorting channel with two magnets. The trajectories in the chip are calculated with COMSOL, images are made with fluorescence microscopy. Colors of trajectories match with colors of cells.

With three magnets, we can see a similar movement for the LNCAP's as in the previous situations, as shown in Figure 33a. In the middle of the channel Figure 33b, we can see a separated flow of PC3-9 cells and LCL cells. In both the model as the experiments it is visible that EpCAM low cells are caught in the channel closest to the magnet (Figure 33c). In the experiment however, the few PC3-9 cells which end up in the waste channel are caught on the wall (Figure 33d).

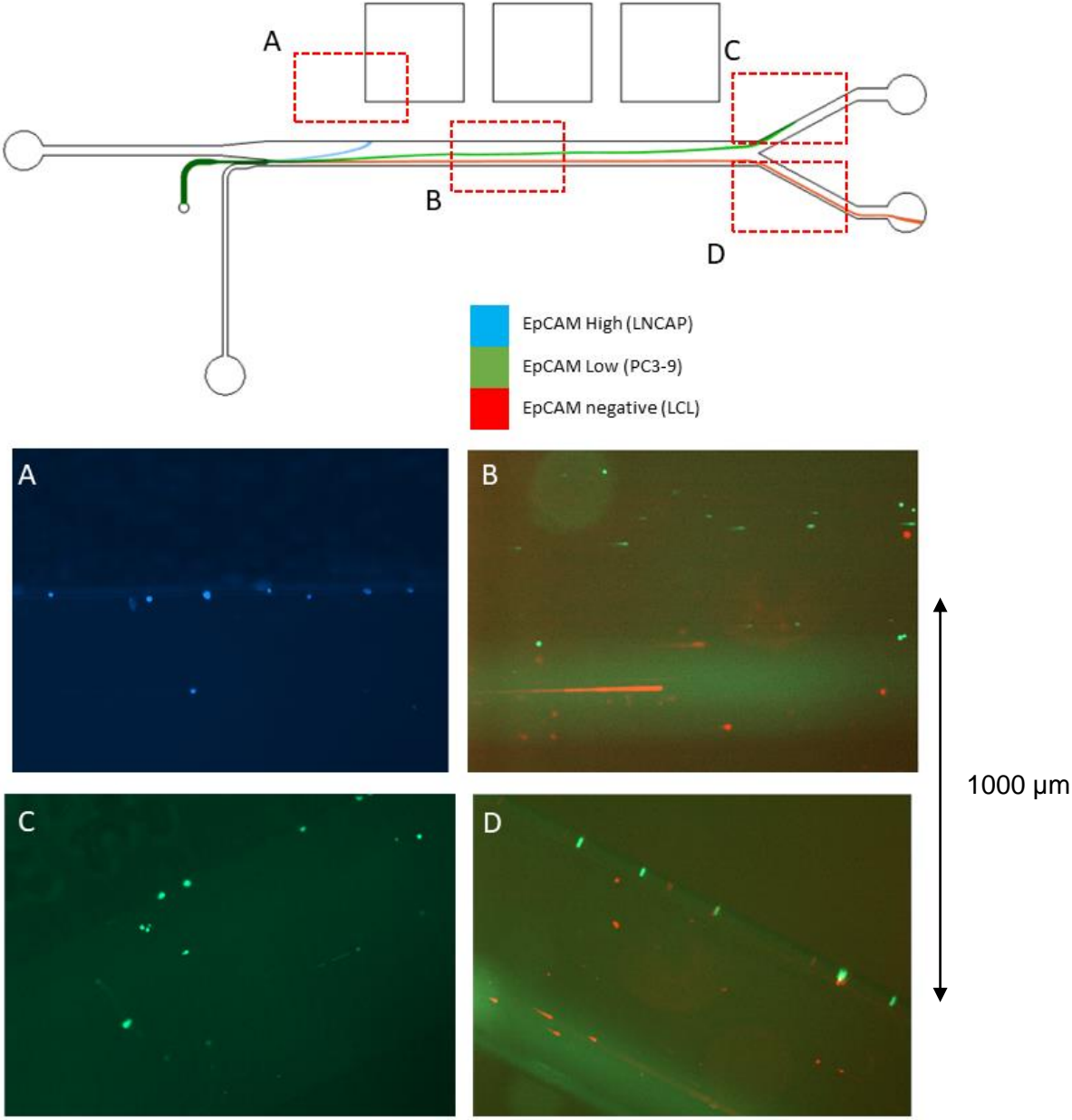


Figure 33: Results of calculating and imaging trajectories of EpCAM high, EpCAM low and EpCAM negative cells in the sorting channel with three magnets. The trajectories in the chip are calculated with COMSOL, images are made with fluorescence microscopy. Colors of trajectories match with colors of cells.

This experiment shows that for the creation of clear, separate fractions, more magnetic attraction is not always better. In this case, use of 1 or 2 magnets might be sufficient for the goal of capturing EpCAM high cells in the chip while also separating EpCAM low and EpCAM negative cells, as with 3 magnets there is also a fraction caught in the waste channel. Furthermore, the experimental results show a very large spread in magnetic moment of PC3-9 cells. Cells of this population end up in each fraction, which shows a difficulty in magnetically sorting these cells.

3.3.3. Cell sorting based on magnetic moment

The retrieval of different populations of cells was unsuccessful, as visible in Figure 34. There is a very large overlap between the different populations and there are in no way distinct groups of cells visible. This is problematic as this means that at this moment, the chip can not be used to actually process samples into different populations. There is a slight relation visible between average PE intensity and population, with the caught fraction being the highest and the waste being the lowest, but the difference is small.

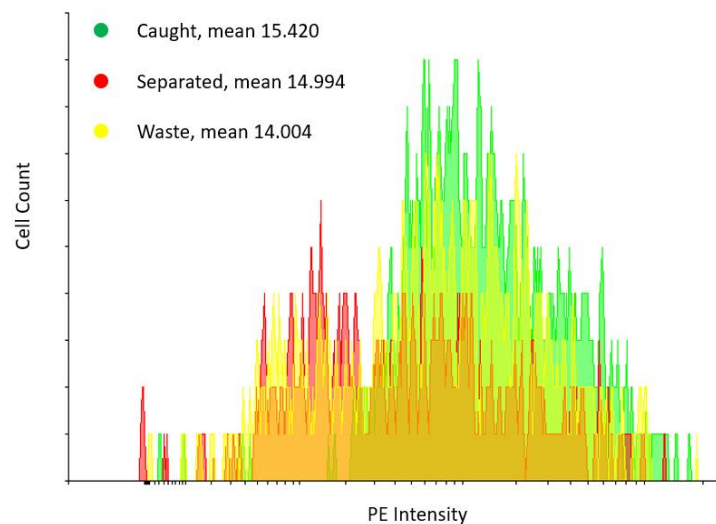
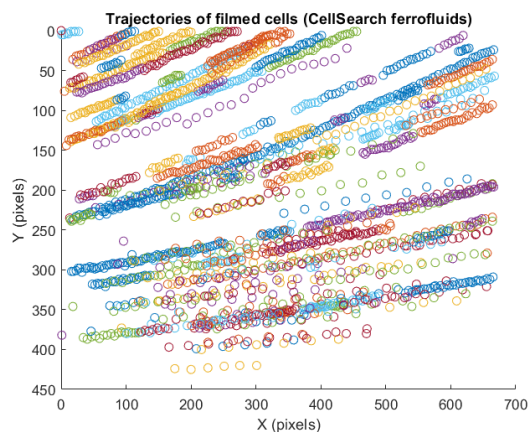


Figure 34: Overlay histograms of PE intensities from cells in different populations after sorting with Chip V2. Graph made with flowing software.

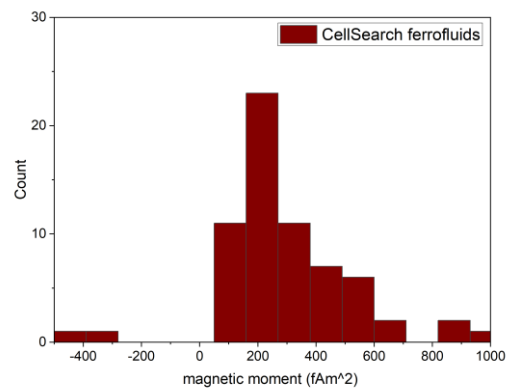
3.3.4 Velocimetry

By imaging the trajectories of LNCAP's stained with different types of ferrofluids resulted in clear differences in pathways. This is visible on the video's, which are available on YouTube (<https://youtu.be/SKAmxpU68IQ>). The CellTracker script could successfully track these cells through the video, as shown in Figure 35.

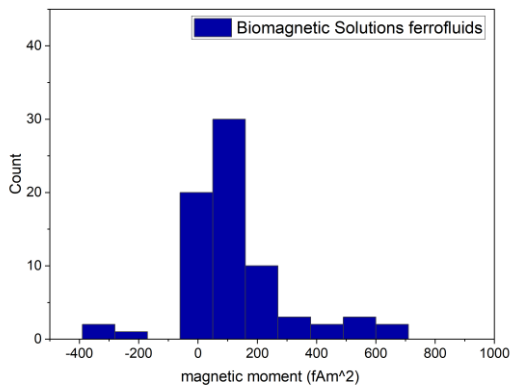
Using the velocimetry part of the CellTracker script, we can translate these trajectories into magnetic moments of the imaged cells. These are shown in Figure 35. Here it is visible that the magnetic moments of cells incubated with CellSearch ferrofluids or Biomagnetic Solutions ferrofluids are higher than those stained with the in house produced ferrofluids. It is also visible that some cells show negative magnetic moments. This happens when a cell has a trajectory oriented away from the magnet. From a physics' point of view, a negative magnetic moment does not make sense and these cells can be considered to have a magnetic moment equal to zero.



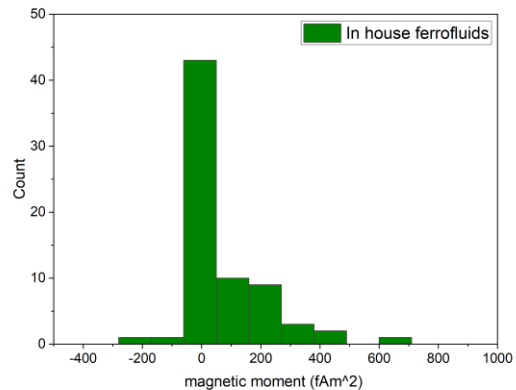
a. The trajectories of LNCAPs incubated with CellSearch ferrofluids. The axes represent locations of pixels in the image.



b. The magnetic moment of LNCAP cells coated with CellSearch ferrofluids



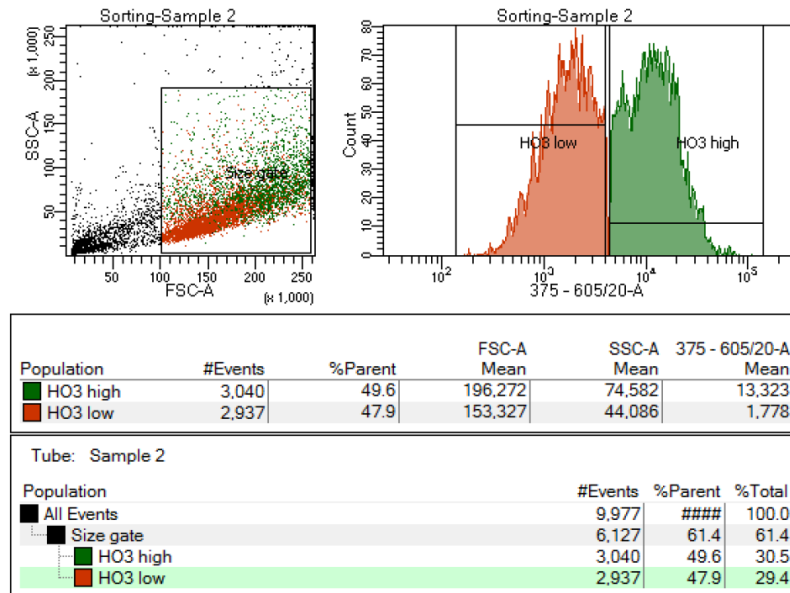
c. The magnetic moment of LNCAP cells coated with Biomagnetic Solutions ferrofluids.



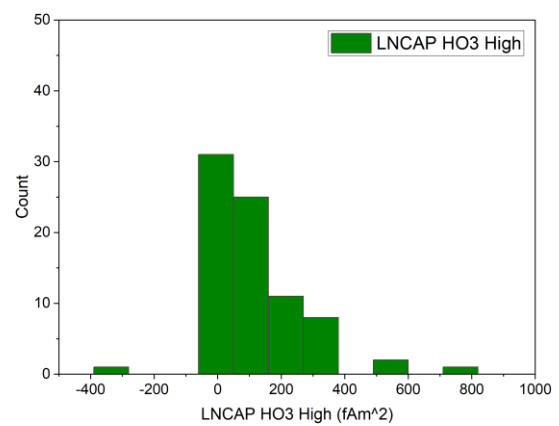
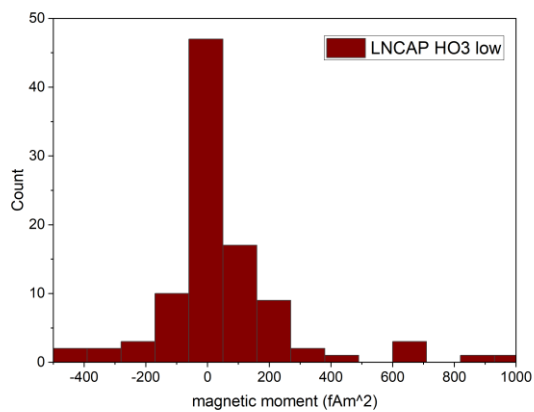
d. The magnetic moment of LNCAP cells coated with the in house produced ferrofluids.

Figure 35: The trajectories of LNCAPs incubated with CellSearch ferrofluids. Cells were filmed while flowing through Chip V3. The axes represent locations of pixels in the image.

For investigating the relation between EpCAM expression and magnetic moment cells were first sorted on their HO3 BV605 fluorescence intensity as shown in Figure 36a. After incubation with 10 $\mu\text{g}/\text{ml}$ of CellSearch ferrofluid, the HO3 high population showed a higher average magnetic moment than their HO3 low counterpart. The magnetic moment of these cells was lower than in Figure 35b however, which were similar cells.



a. FACS plots of sorting LNCAP cells based on their HO3 expression. Cells in the red and green populations were collected separately.



b. Calculated magnetic moments of the LNCAP HO3 low population using image velocimetry.

c. Calculated magnetic moments of the LNCAP HO3 high population using image velocimetry.

Figure 36: Results of image velocimetry on EpCAM high and EpCAM low populations of LNCAP cells.

3.4 Discussion

3.4.1 Flow focusing

When comparing the chip oriented perpendicular to gravity to the chip oriented parallel to gravity, it is interesting to observe that while the perpendicular orientation produces a spatially more focused cell stream, the percentual spread does not differ between the two orientations. For accurate sorting, it is the percentual spread in cell velocity that should be as low as possible. As this is similar in both orientations, it can be concluded that the orientation is not a factor of importance and that the orientation which is the most practical can be used. For the experiments in this thesis, this will be the perpendicular orientation as this allows for easier imaging.

In chip version 2, cells are better focused but touch the wall which might damage fragile CTC's. In version 3, the cells are better suspended and move more freely in the channel, however the level of focus decreases. The flow focusing in the chip shows a very strong analogy with FACS sorting. It is widely known in flow cytometry that a high sheath flow to sample ratio is required to get cells flowing in a nice single file [38]. In the theoretical model of Williams et al., it was found that a sample to sheath flow ratio of 0.04:1 was optimal, and ratios between 0.03 and 0.05 to 1 were acceptable. With the tested ratios, the best performing ratio was indeed in this range (0.05 to 1). Even with optimal settings, the chip was not able to have cells streaming in a single file however. To be able to focus even better, without cells rolling on the wall, a new chip design with a smaller inlet channel might help.

3.4.2 Magnetic configuration

Regarding the testing of the different magnetic setups, it is important to notice that the found optimal magnetic configuration is only valid for these chip dimensions, flow rate and cell populations. Creating distinct groups is a very delicate process as different populations of cells might overlap in their magnetic moment. Also, the required recovery rate and depletion rate might differ from patient to patient. It is imaginable that for screening patients with non-metastatic disease a high recovery rate is more important than a high depletion. This would require high magnetic attraction. For patients with late stage carcinoma's however a higher depletion is more important, as they have more CTC's and a sample with higher purity is better for downstream analysis. This ability to shift sensitivity based on what is expected and required from different patients can be seen as a strength of the system.

It seems that the modeled sorting chip of Williams et al. showed very distinct separation of different groups of cells, much like the COMSOL model did for the three populations of cells which we used [33]. The goal of their chip is to separate for example CTC's from circulating Cancer Stem Cells (CSC's), which should have lower EpCAM expression [33]. Based on the fact that in our results, especially EpCAM low cells showed a wide spread over the different fractions, it can be expected that attempting to separate cells over 6 fractions with different types of cells will be quite difficult. Thus, completely separating CSC's from other types of EpCAM Low CTC's based on their magnetic moment alone is probably not doable and other downstream techniques should be applied to identify these cells, which raises the question whether a 6-channel sorting system is required at all.

Furthermore, it will be very hard to attract EpCAM high cells in a way that they are separated, but not caught in the channel, while also being able to separate EpCAM low cells. These EpCAM high cells might be several orders in magnitude higher in magnetic moment than less positive cells. Solsona et al ([35]) acknowledge this problem and, similar to our approach, defined a fraction of particles caught on chip. Jack et al (2017) have a very similar device to ours, but use it in two sequential steps [39]. The system is shown in Figure 38. In the first step, they flow the sample through with a magnet far from the chip, such that only the EpCAM high cells are separated. In the secondary step, they flow the sample through a similar device, but now with the magnet closer to the channel, such that EpCAM low cells are now likewise separated; a method which is also easily applicable on the fine separation device.

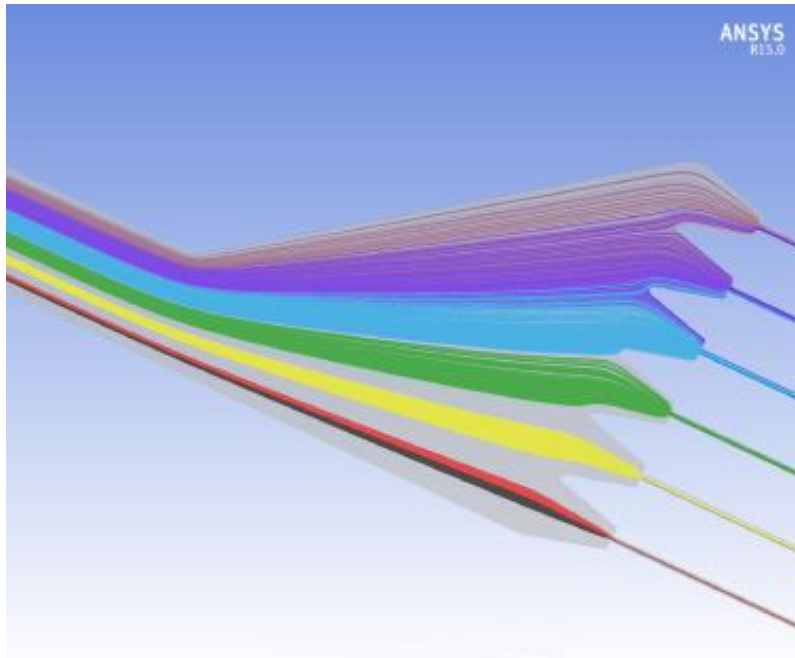


Figure 37: Trajectories of cells in model of Williams et al. Cells are attracted by a magnet which is placed out of view. Visible are very distinct fractions of cells with little overlap. Image from [33].

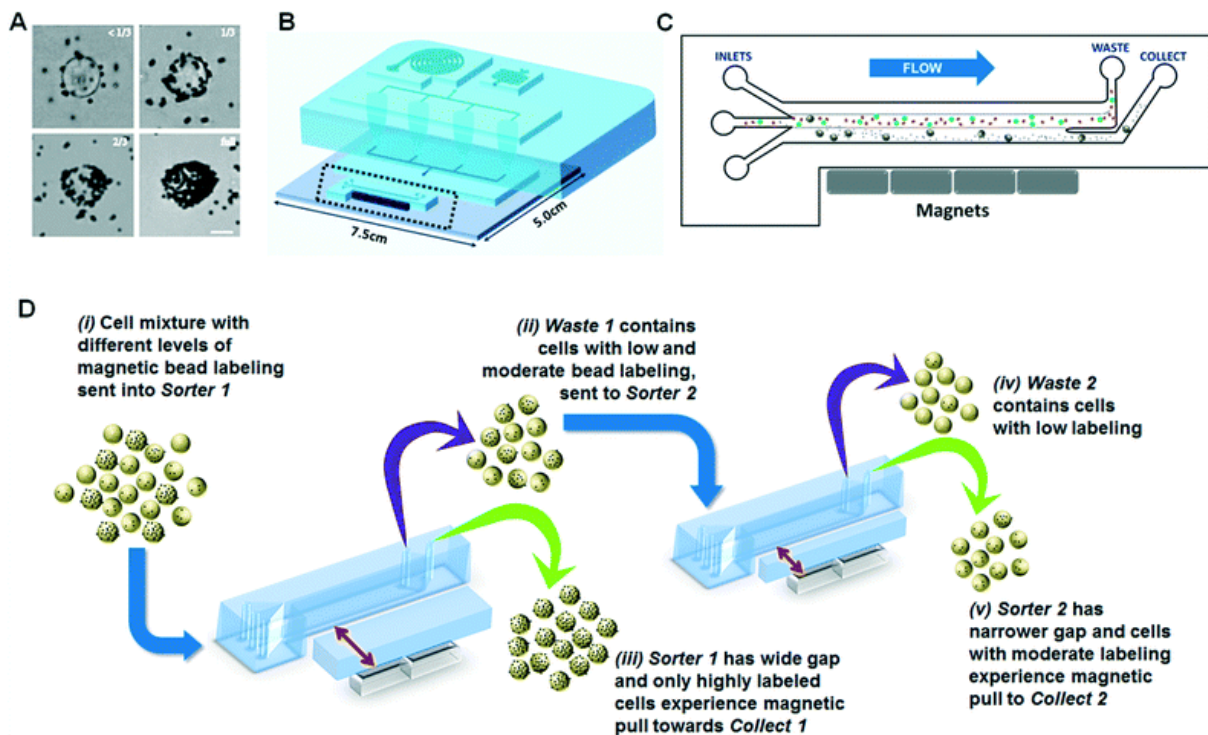


Figure 38: The sorting device of Jack et al. The same microfluidic system is applied twice in a row, once with a wide gap between magnet and channel and once with a narrow gap. Image from [39].

3.4.3 Cell sorting based on magnetic moment

Although we can see from the trajectories of the cells that we are creating distinct populations in the channel, we are not able to retrieve the sorted cells as such. The inability to retrieve the sorted cells as populations is problematic as this renders the chip useless for processing samples at the moment. There is no simple solution to this problem. Some things which are encountered during flow might result in disturbance of the population:

- Air bubbles disturb flow and move cells
- Due to very low flow rates, the flow is unstable and therefore very sensitive to disturbances
- The 4 mm wide luer-outlets are relatively wide in comparison to the channels and create dead-flow zones in which cells get stuck
- Cells have to move against gravity to leave the channel, which is problematic at low flow rates as they will sedate on the lowest point

Unfortunately, most of these problems can not be solved by using different methods to operate the chip but require real changes in design. We will later propose some alterations which might solve these issues.

3.4.4 Particle image velocimetry for measuring magnetic moment

We were able to compare different types of ferrofluids using image velocimetry and retrieve quantitative data on the magnetic moments of the different cells. The problem is however that there is no control to check whether the calculated magnetic moments are correct. The only method to validate the image velocimetry technique is to perform measurements on particles with known magnetic moments. For now we can state that the order of magnitude of the calculated moments is in compliance with earlier experiments, as we know from COMSOL simulations performed for the rough separation that PC3-9 cells coated with CellSearch ferrofluids have moments between 0-60 fAm² and LNCAP cells should be higher than that.

We were also able to relate the EpCAM expression of cells with their magnetic moment by first sorting on HO3 expression and performing the image velocimetry right after. The EpCAM high population showed lower moments than the LNCAP's cells showed before however. This might be due to antibody cross-blocking as the HO3 epitope and the VU1D9 epitope, which is targeted by the CellSearch ferrofluid, are close to each other.

3.5 Conclusion

To conclude, a new microfluidic device was designed to deflect cells into three populations based on their magnetic moment. Three iterations were performed to get to the final device, which was able to separate LNCAP cells, PC3-9 cells and LNCAP cells. In this device, cells are focused by injecting the sample between two sheath buffer streams at a ratio of 0.05:1. The use of one or two 10x10x35 mm³ N52 block magnets was enough to have an adequate separation in the channel.

Actually retrieving the separated fractions was not successful and additional work on this has to be performed in order to make the fine separation applicable in laboratory practice. We could however use the chip to retrieve data on the magnetic properties of cells in the channel by using image velocimetry.

In the next chapter we will put the rough and fine separation in a clinical perspective, how can we apply what was learnt to the processing of DLA product and in a Cancer Watch?

4. The clinical perspective

4.1 Diagnostic Leukapheresis Product

The rough separation setup is optimized with processing DLA product in mind. With the optimal configuration, the protocol for processing a 60ml DLA sample using Ibidi chips looks like this (Table 5):

Step	Action
1	Incubate DLA sample with ferrofluids
2	Treat 600 μm chip with Casein buffer (15 min)
3	Flush through sample at .5 ml/min, separate using optimized Halbach array
4	Rinse with 2 ml of Casein buffer at .5 ml/min
5	Wash with 4 ml of Casein buffer at 2 ml/min
6	Remove magnet
7	Flush out separated fraction (1 ml air- 1 ml Casein buffer – 1 ml air – 1ml Casein buffer – 1ml air)

Table 5: Protocol for processing DLA product with Ibidi chips

This protocol is used with only one chip and would take over 2 hours. Performing this protocol with three chips in parallel would bring this down to 40 minutes. The enriched samples are not ready for enumeration however, as they are not stained. Staining would take at least 30 minutes and could be performed on chip. For on chip staining, the staining buffer can be flown in the channel while the cells are stuck to the magnet. When the buffer is in place, the magnet can even temporarily be removed to allow for mixing. For washing away unbound antibodies, the magnet can be attached again such that no unnecessary cell loss occurs. The stained cells can even be enumerated within the channel as the Ibidi chips are designed to be imaged.

One problem of processing large samples which is not considered yet is that the presence of the large amounts of ferrofluids might influence the effectiveness of fluorescence microscopy. It was found that the amount of ferrofluids in a CellSearch sample (13 μg) can lead to a 11-67% reduction of fluorescence signal [40]. As processing a full 60 ml sample would lead to an accumulation of 200 μg of nanoparticles in the channel, one could easily imagine what this would do to the fluorescent signal. For CellSearch samples it was already shown that washing of the sample using centrifugation can decrease the amount of free ferrofluids with 96% [40].

The fine separation is not yet ready to be applied on DLA samples. While it was able to deflect cells into different populations, it was not able to retrieve these populations as such. The sorting chip is now tested to be used with a sample flow ratio of 2 $\mu\text{l}/\text{min}$, with concentrations ranging up to 300 cells per μl . Assuming that the input volume of the fine separation would be the same size as a CellSearch sample, which is 300 μl , it would take 2.5 hours to process this sample. With the same throughput, around 100 000 cells can be processed in this 300 μl sample.

4.2 Towards a Cancer watch

The work in this thesis has shown that it is very much feasible to enrich CTC's using in flow immunomagnetophoresis. The question is, how can we translate this towards a device which can process blood in a apheresis-like manner? Thus; retrieving blood from a patient and pumping the CTC-depleted fraction back. In apheresis, blood is retrieved from a patient and then fractionated. Broadly speaking, there are two methods to do so; either using continuous flow or intermittent flow [41].

Continuous flow systems are continuously both withdrawing and injecting blood. A continuous flow exist from patient – to separator – to patient [42]. **Intermittent flow** systems withdraw and process blood in batches, which are then injected over the same line as they were retrieved from. Continuous flow systems have the advantage that they are faster, but, from an engineer's point of view, pose more challenges [43].

A very simple version of a CTC-apheresis setup would look something like Figure 39. This intermittent flow system draws blood from a patient, which is processed through a CTC enrichment device. The CTC-depleted blood is retrieved in a blood transfusion IV bag and injected back into the patient with an ordinary drip IV. After the first withdrawn batch is processed, withdrawal and injection can be performed simultaneously using two separate venipunctures.

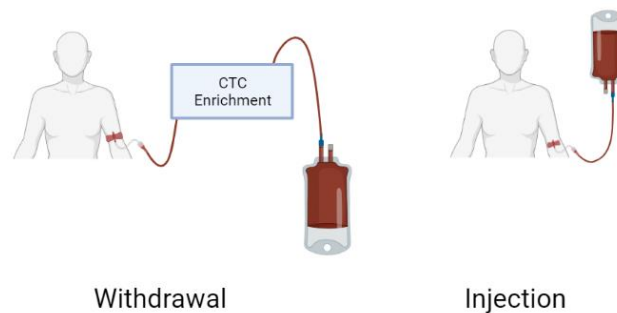


Figure 39: A rudimentary version of a CTC-apheresis setup. First, blood is drawn from a patient, flown through a separation device and collected in an IV bag. The CTC-depleted blood is then transfused back into the patient with an ordinary drip IV.

Kang et al (2014) demonstrated the ability to immunomagnetically filter pathogens from blood of rats with sepsis using a extra-corporeal blood cleansing device which they have modelled to work like a human spleen [44]. This continuous flow device works similar to the fine separation device, only with an additional filter between waste and separated outlets [45]. Like our setup, they utilize streptavidin-coated superparamagnetic beads which bind to the targeted cells.

One problem that has not been solved in this thesis and is of importance in a flow based CTC enrichment system is the ferrofluid incubation step. This is a time-consuming step which is now performed statically, in magnetic fields [30, 46, 47]. Some work is already performed on in flow incubation of particles with ferrofluids. Kang et al. solve this problem by continuously injecting ferrofluids into flowing whole blood, which is mixed using a Kenics inline mixer. The incubation is then performed for 10 min by flowing the sample through series of helically looped tubing. Kim et al (2007, [48]) propose a method in which they use magnets to pull ferrofluids into a sample stream, as visible in Figure 40. It is also possible to use magnetic fields which create clouds of ferrofluids, which a target has to pass through. This is performed by Lacharme et al (2009, [49]) who use this to capture antibodies.

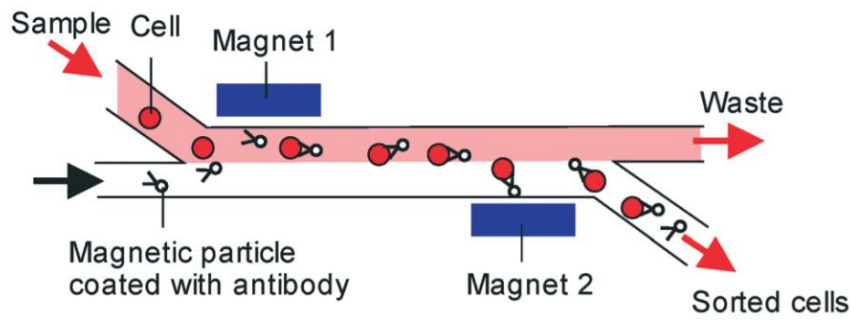


Figure 40: In flow magnetic incubation, cells are flown in a sample stream and ferrofluids are magnetically pulled close for incubation. Image by [50] which is a reproduction from.

The use of very large amounts of ferrofluids are required to process large amounts of sample. Depending on the type of particle used, cost of ferrofluids for processing a full 5L whole blood sample will be in the € 50 000- 100 000 range [51-53]. Stevens et al. demonstrated the possibility to reuse ferrofluids in a concept they have called ‘reFLECT-CTC’ [54]. In their setup, unbound ferrofluids are recycled and incubated with a fresh portion of sample. Figure 41 shows a possible reFLECT-CTC configuration. The rough separation setup with Ibidi μ -slides is directly applicable in this concept for capture of CTC’s and ferrofluids.

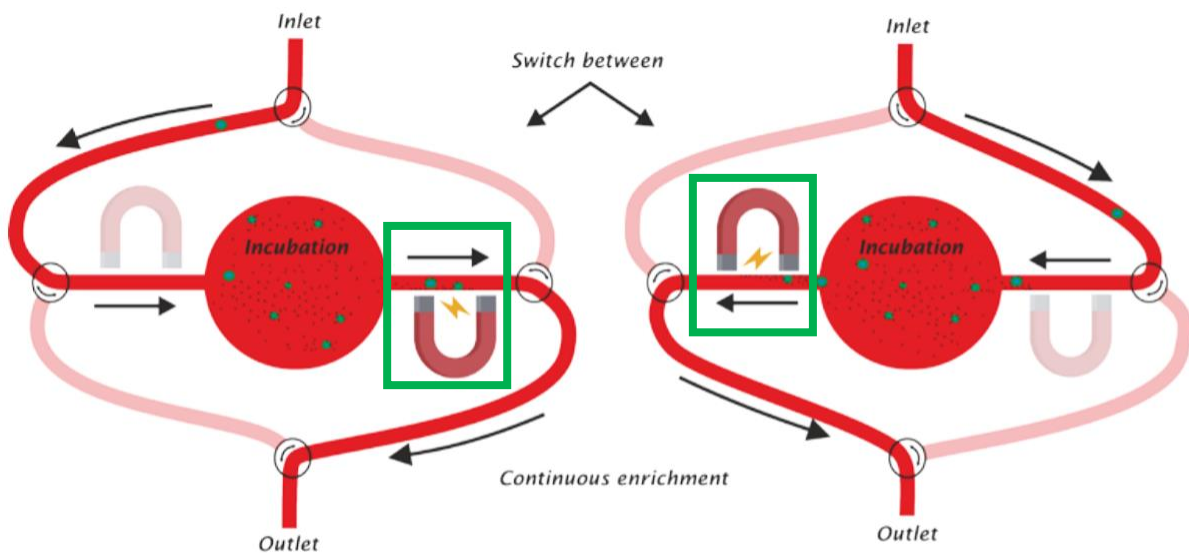


Figure 41: A version of the reFLECT-CTC concept of Stevens et al. Ferrofluids are flown back and forth two magnet arrays while continuously being incubated with fresh sample. The green square shows where the rough separation configuration would be applied. Image is an adaptation of patent [54].

5. Recommendations

5.1 Rough separation

While we attempted to get a full picture of the rough separation, there are still some questions unanswered. Therefore there are some recommendations on how to proceed with this project:

The effect of placing the chips in parallel can also be reached by using a chip with a wider channel. This would have the advantage that less tubing and therefore less fluid volume is necessary to build a full system. The problem however is that such a chip probably is not available commercially and should be designed, which is costly.

Although a lot can be learned from the model samples used in this thesis, they will never be a substitute for patient material. Real clinical DLA samples will contain lots of cells, platelets and proteins which have not been accounted for in this thesis. These objects might interact with the chip, the ferrofluids or each other and this can influence the performance of the separation. Testing the rough separation setup with patient material is a logical next step. This can both be with spiked cells in healthy donor samples or with patient material.

As the ultimate goal is to build a Cancer Watch, it would also be interesting to build the flow switching concept of reFLECT CTC. A simple proof of principle setup would not be that hard to build and can demonstrate the concept.

5.2 Fine separation

One problem which was encountered with fine separation is that it was hard to retrieve cells from the chip. It is not entirely clear why this is so, but the design can definitely be improved to work towards a solution. The outlets of the chip, for instance, are relatively wide in comparison to the rest of the device. Because of this, the flow rate significantly drops on a point where cells have to move against gravity to get out of the chip. One proposition to solve this problem is shown in Figure 42. This design utilizes needles for the connection between chip and tubing. These needles are placed in plane with the channel, such that the problem of going against gravity at low flow speed is avoided.

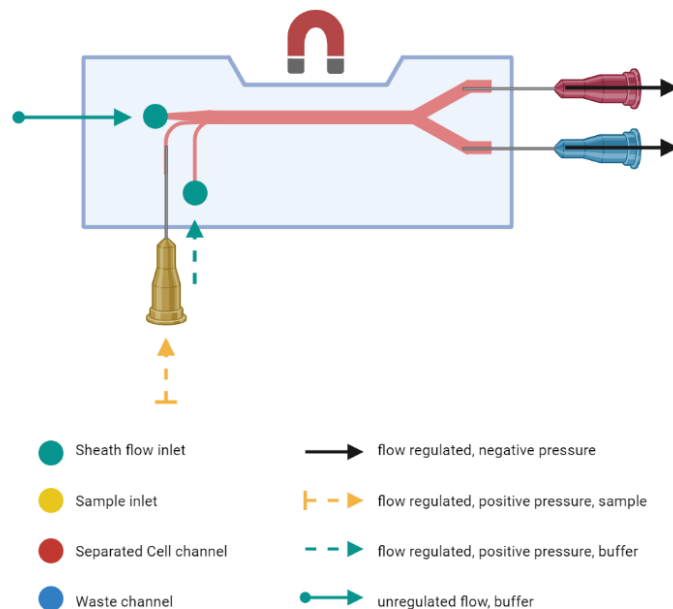


Figure 42: A schematic view of a proposed chip V4, with needle based sample inlets and outlets. The sample is injected and withdrawn from the stream with needles which are placed in the same plane as the channel.

Using flow focusing, we were able to get a stream of sample which was about as wide as the inlet channel. To get even narrower streams, it might be possible to utilize small capillary needles, such as those used in IVF (in vitro fertilization) for example. This is difficult to apply using the current production technique of micro-milling but with soft-lithography for example one could cast PDMS around the capillary such that it is embedded in the channel.

The velocimetry measurements are now performed with chip V3. While this is possible, this might not be the optimal configuration for such a system. It is advisable to design a new iteration of V3, with only one outlet channel and a decreased sorting channel width, such that the whole width of the channel is imageable. A schematic design of such a device is shown in Figure 43.

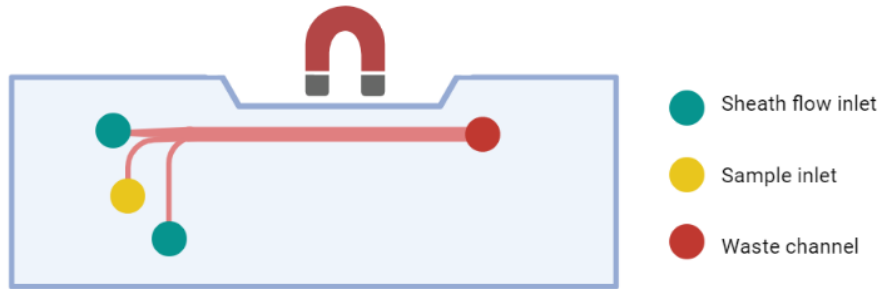


Figure 43: Proposed image velocimetry device, with similar operations as chip V3 but with one outlet except 2.

6. Acknowledgements

I like to thank my daily supervisor Michiel Stevens for all his help with my thesis. The amount of time and effort he spent on my project was nothing like I have encountered before from any kind of supervisor and I really appreciate this. I'd also like to thank Leon Terstappen for his generous help. The connections he made for me have shaped the beginning of my career and are extremely appreciated.

From the BIOS group I'd like to thank Jeroen Vollenbroek for his help with producing the various versions of the fine separation chip. His expertise on microfluidic devices was very useful. Furthermore I'd like to thank Mathieu Odijk for being my external supervisor and Eiko Westerbeek for taking time to sit with me discussing the image velocimetry part.

My appreciation goes out to everybody on the Cancer Watch project for providing me with their insights and expertise during our bi-weekly meetings. I am very interested in how this project will progress and hope the Cancer Watch will one day reach it's full potential.

Figures 1, 2, 5, 7, 17, 20, 39, 42 and 43 are made with BioRender under a student licence. Figure 26 is made with lucichart and Figure 34 is made with Flowing Software for FACS data.

7. Resources

1. Gambardella, V., et al., *Personalized Medicine: Recent Progress in Cancer Therapy*. *Cancers*, 2020. **12**(4): p. 1009.
2. Verma, M., *Personalized medicine and cancer*. *J Pers Med*, 2012. **2**(1): p. 1-14.
3. Krzyszczyk, P., et al., *The growing role of precision and personalized medicine for cancer treatment*. *Technology*, 2018. **6**(3-4): p. 79-100.
4. Li, S.G. and L. Li, *Targeted therapy in HER2-positive breast cancer*. *Biomed Rep*, 2013. **1**(4): p. 499-505.
5. Porru, M., et al., *Targeting KRAS in metastatic colorectal cancer: current strategies and emerging opportunities*. *J Exp Clin Cancer Res*, 2018. **37**(1): p. 57.
6. Tellez-Gabriel, M., M.-F. Heymann, and D. Heymann, *Circulating Tumor Cells as a Tool for Assessing Tumor Heterogeneity*. *Theranostics*, 2019. **9**(16): p. 4580-4594.
7. Chen, Y., et al., *Circulating tumor cells undergoing EMT are poorly correlated with clinical stages or predictive of recurrence in hepatocellular carcinoma*. *Scientific Reports*, 2019. **9**(1): p. 7084.
8. de Wit, S., et al., *EpCAM(high) and EpCAM(low) circulating tumor cells in metastatic prostate and breast cancer patients*. *Oncotarget*, 2018. **9**(86): p. 35705-35716.
9. Jie, X.-X., X.-Y. Zhang, and C.-J. Xu, *Epithelial-to-mesenchymal transition, circulating tumor cells and cancer metastasis: Mechanisms and clinical applications*. *Oncotarget*, 2017. **8**(46): p. 81558-81571.
10. Swennenhuis, J.F., et al., *Efficiency of whole genome amplification of single circulating tumor cells enriched by CellSearch and sorted by FACS*. *Genome Medicine*, 2013. **5**(11): p. 106.
11. Stevens, M., et al., *VyCAP's puncher technology for single cell identification, isolation, and analysis*. *Cytometry Part A*, 2018. **93**(12): p. 1255-1259.
12. Toss, A., et al., *CTC enumeration and characterization: moving toward personalized medicine*. *Ann Transl Med*, 2014. **2**(11): p. 108.
13. Coumans, F. and L. Terstappen, *Detection and Characterization of Circulating Tumor Cells by the CellSearch Approach*. *Methods Mol Biol*, 2015. **1347**: p. 263-78.
14. Technology, S. *RosetteSep™ CTC Enrichment Cocktail Containing Anti-CD36 Product information*. 2019 [cited 2020 24-11]; Available from: https://cdn.stemcell.com/media/files/pis/28583-PIS_1_3_1.pdf.
15. Fehm, T.N., et al., *Diagnostic leukapheresis for CTC analysis in breast cancer patients: CTC frequency, clinical experiences and recommendations for standardized reporting*. *Cytometry A*, 2018. **93**(12): p. 1213-1219.
16. Andree, K.C., et al., *Toward a real liquid biopsy in metastatic breast and prostate cancer: Diagnostic LeukApheresis increases CTC yields in a European prospective multicenter study (CTCTrap)*. *Int J Cancer*, 2018. **143**(10): p. 2584-2591.
17. Stoecklein, N.H., et al., *Challenges for CTC-based liquid biopsies: low CTC frequency and diagnostic leukapheresis as a potential solution*. *Expert Review of Molecular Diagnostics*, 2016. **16**(2): p. 147-164.
18. Hoshino, K., et al., *Microchip-based immunomagnetic detection of circulating tumor cells*. *Lab on a chip*, 2011. **11**(20): p. 3449-3457.
19. Smith, J.P., et al., *Microfluidic transport in microdevices for rare cell capture*. *Electrophoresis*, 2012. **33**(21): p. 3133-42.
20. Liu, P., et al., *Magnetic Particles for CTC Enrichment*. *Cancers*, 2020. **12**(12): p. 3525.
21. Stevens, M., et al., *Optimal Halbach Configuration for Flow-through Immunomagnetic CTC Enrichment*. *Diagnostics*, 2021. **11**(6): p. 1020.

22. Jalali, M., et al., *Electromagnetic shielding of polymer–matrix composites with metallic nanoparticles*. Composites Part B: Engineering, 2011. **42**(6): p. 1420-1426.
23. Bruus, H., *Theoretical Microfluidics*. 2008.
24. Liberti, P.A., C.G. Rao, and L.W.M.M. Terstappen, *Optimization of ferrofluids and protocols for the enrichment of breast tumor cells in blood*. Journal of Magnetism and Magnetic Materials, 2001. **225**(1): p. 301-307.
25. Tibbe, A.G.J., et al., *Magnetic field design for selecting and aligning immunomagnetic labeled cells*. Cytometry, 2002. **47**(3): p. 163-172.
26. Thermofisher-scientific. *Blocker™ Casein in PBS product page*. [cited 2021 28-4]; Available from: <https://www.thermofisher.com/order/catalog/product/37528#/37528>.
27. Liu, W. and C.-Y. Wu, *Modelling Complex Particle–Fluid Flow with a Discrete Element Method Coupled with Lattice Boltzmann Methods (DEM-LBM)*. ChemEngineering, 2020. **4**(4): p. 55.
28. Nicolazzo, C., et al., *EpCAM^{low} Circulating Tumor Cells: Gold in the Waste*. Disease Markers, 2019. **2019**: p. 1718920.
29. Wit, S.d., et al., *The detection of EpCAM+ and EpCAM– circulating tumor cells*. Scientific Reports, 2015. **5**(1): p. 12270.
30. Terstappen, L.W., *Methods for enhancing binding interactions between members of specific binding pairs*, L. VERIDEX, Editor. 2003: United States.
31. Smith, J., et al., *Feasibility of single-cell analysis of model cancer and foetal cells in blood after isolation by cell picking*. Tumour Biol, 2019. **41**(2): p. 1010428318823361.
32. Di Trapani, M., N. Manaresi, and G. Medoro, *DEPArray™ system: An automatic image-based sorter for isolation of pure circulating tumor cells*. Cytometry Part A, 2018. **93**(12): p. 1260-1266.
33. Williams, P.S., et al., *Microfluidic chip for graduated magnetic separation of circulating tumor cells by their epithelial cell adhesion molecule expression and magnetic nanoparticle binding*. Journal of Chromatography A, 2021. **1637**: p. 461823.
34. Ozkumur, E., et al., *Inertial focusing for tumor antigen-dependent and -independent sorting of rare circulating tumor cells*. Science translational medicine, 2013. **5**(179): p. 179ra47-179ra47.
35. Solsona, M., et al., *Magnetophoretic Sorting of Single Catalyst Particles*. Angew Chem Int Ed Engl, 2018. **57**(33): p. 10589-10594.
36. Reddy, S., et al., *Determination of the magnetic susceptibility of labeled particles by video imaging*. Chemical Engineering Science, 1996. **51**(6): p. 947-956.
37. Chalmers, J.J., et al., *Quantification of cellular properties from external fields and resulting induced velocity: Cellular hydrodynamic diameter*. Biotechnology and Bioengineering, 1999. **64**(5): p. 509-518.
38. Biotec, M. *Flow cytometry basics*. [cited 2021 21-6]; Available from: <https://www.miltenyibiotec.com/DE-en/resources/macshandbook/macstechnologies/flow-cytometry/flow-cytometry-basics.html>.
39. Jack, R., et al., *Microfluidic continuum sorting of sub-populations of tumor cells via surface antibody expression levels*. Lab on a Chip, 2017. **17**(7): p. 1349-1358.
40. Scholtens, T., et al., *Automated identification of circulating tumor cells by image cytometry*. Cytometry. Part A : the journal of the International Society for Analytical Cytology, 2012. **81**: p. 138-48.
41. Burgstaler, E.A. and A.A. Pineda, *Therapeutic cytopheresis: Continuous flow versus intermittent flow apheresis systems*. Journal of Clinical Apheresis, 1994. **9**(4): p. 205-209.
42. Higuchi, A., *3.11 - Separation and Purification of Stem and Blood Cells by Porous Polymeric Membranes*, in *Comprehensive Membrane Science and Engineering*, E. Drioli and L. Giorno, Editors. 2010, Elsevier: Oxford. p. 253-276.

43. Hitzler, W., et al., *Comparison of intermittent- and continuous-flow cell separators for the collection of autologous peripheral blood progenitor cells in patients with hematologic malignancies*. *Transfusion*, 2001. **41**: p. 1562-1566.
44. Kang, J.H., et al., *An extracorporeal blood-cleansing device for sepsis therapy*. *Nature Medicine*, 2014. **20**(10): p. 1211-1216.
45. Yung, C.W., et al., *Micromagnetic–microfluidic blood cleansing device*. *Lab on a Chip*, 2009. **9**(9): p. 1171-1177.
46. Coumans, F., G. van Dalum, and L.W.M.M. Terstappen, *CTC Technologies and Tools*. *Cytometry Part A*, 2018. **93**(12): p. 1197-1201.
47. Swennenhuis, J.F., et al., *Improving the CellSearch® system*. *Expert Rev Mol Diagn*, 2016. **16**(12): p. 1291-1305.
48. Kim, J., et al. *Development of a novel micro immune-magnetophoresis cell sorter*. in *SENSORS, 2007 IEEE*. 2007.
49. Lacharme, F., C. Vandevyver, and M.A.M. Gijs, *Magnetic beads retention device for sandwich immunoassay: comparison of off-chip and on-chip antibody incubation*. *Microfluidics and Nanofluidics*, 2009. **7**(4): p. 479.
50. Hejazian, M., W. Li, and N.T. Nguyen, *Lab on a chip for continuous-flow magnetic cell separation*. *Lab Chip*, 2015. **15**(4): p. 959-70.
51. Biotec, M. *product page Streptavidin MicroBeads*. [cited 2021 28-5]; Available from: <https://www.miltenyibiotec.com/DE-en/products/streptavidin-microbeads.html#for-1x10-sup-9-sup-total-cells>.
52. iMag, B. *product Page Streptavidin Particles Plus - DM* [cited 2021 28-5]; Available from: <https://www.bdbiosciences.com/eu/reagents/research/magnetic-cell-separation/other-species-cell-separation-reagents/streptavidin-particles-plus---dm/p/557812#>.
53. Thermofisher-scientific. *Product page Dynabeads™ M-270 Streptavidin*. [cited 2021 28-5]; Available from: <https://www.thermofisher.com/order/catalog/product/65305#/65305>.
54. Stevens, M., *Device and Method For The Continuous Trapping of Circulating Tumor Cells*, U.o. Twente, Editor. 2020: United States of America.

Appendix A: Supplementary to physics

A.1 Derivation of the flow field

As we operate a flow rate controlled system, we want to define the flow field based on a certain flow rate. To derive this, we start with the formula for a pressure driven parabolic flow field, as found in Bruus et al [23].

$$v(x) = \frac{1}{2\eta} (x^2 - a^2) \frac{dP}{dy} \quad (1)$$

With v the flow speed (m/s), η the viscosity (Pa/s), x the location on the vertical axis (m, $x = 0$ at the middle of the channel), a half the height of the channel (m) and $\frac{dP}{dy}$ the pressure difference per unit of length of the channel (Pa/m). Viscosity, channel height and pressure difference can all be considered as constants. Then you get simple second degree polynomial which means that the flow profile is parabolic. At the edges of the channel $x = a$, thus the flow speed is equal to zero. In the middle of the channel there is a maximum as $x = 0$.

The average flow speed $\langle v \rangle$ (m/s) is equal to the flow rate (Q , m³/s) over the channel area (A , m²).

$$\langle v \rangle = \frac{Q}{A} \quad (2)$$

The formula for pressure difference over a rectangular channel is [23]:

$$\Delta P = \frac{12\eta L \langle v \rangle}{(2a)^2} \quad (3)$$

With ΔP the pressure difference in Pa, η the viscosity (Pa/s), L the length of the channel (m) and a half the height of the channel. As we will later on operate a flow rate controlled pumping system, the pressure should be written out of the model. Substituting $\langle v \rangle$ in (3) for (2) makes:

$$\Delta P = \frac{12\eta L Q}{(2a)^2 A} \quad (4)$$

With dy in (1) equal to channel length L , $dP = \Delta P$ and eq. (4) can be used in eq. (1):

$$v(x) = \frac{3}{2} (x^2 - a^2) \frac{LQ}{Aa^2} \quad (5)$$

As the Area is equal to $2a * w$ with w the width of the channel (m), (5) becomes equation (6), which we can use to describe the flow profile in the channel for a given flow rate:

$$v(x) = \frac{3}{4} (x^2 - a^2) \frac{LQ}{a^3 w} \quad (6)$$

A.2 Extra information on formulas used in MATLAB script

The MATLAB scripts use different formulas to calculate the magnetophoretic force than defined in the physics section. In this part, we show that these are actually the same. In the MATLAB script, the following formula is used:

$$F_{mag} = 2\pi R^3 \mu_0 \frac{\mu_{pr}^{-1}}{\mu_{pr}+2} \nabla(\mathbf{H}^2) \quad (1)$$

With R is the particle radius (m), μ_0 the magnetic permeability of vacuum (N/A^2), μ_{pr} the effective relative magnetic permeability of the cell with ferrofluids (unitless) and ∇H^2 the gradient of the magnetic field squared. μ_{pr} is equal to the effective magnetic permeability of the cell (μ_p , (N/A^2) divided by μ_0). μ_{pr} is dependent on the magnetic moment and can be described using equation (2):

$$\mu_{pr} = 1 + \frac{f(H)*m_{max}}{V_p H} \quad (2)$$

Where,

$$f(H) = \begin{cases} \sqrt{\sin\left(\frac{H}{H_{max}} * \frac{\pi}{2}\right)} & \text{if } H < H_{max} \\ 1 & \text{if } H \geq H_{max} \end{cases} \quad (3)$$

With m_{max} being the maximum magnetic moment of the cell (Am^2), V_p the volume of a particle (m^3) and H_{max} the value of the field at which maximum magnetization is reached. We substitute μ_{pr} in (1) for (2):

$$F_{mag} = 2\pi R^3 \mu_0 \frac{\frac{f(H)*m_{max}}{V_p H}}{\frac{f(H)*m_{max}}{V_p H} + 3} \nabla(\mathbf{H}^2) \quad (4)$$

As $\frac{f(H)*m_{max}}{V_p H} \ll 3$, we can simplify (4) to:

$$F_{mag} = \frac{2}{3} \pi R^3 \mu_0 \frac{f(H)*m_{max}}{V_p H} \nabla(\mathbf{H}^2) \quad (5)$$

V_p is equal to $\frac{4}{3} \pi R^3$. Filling in makes (6):

$$F_{mag} = \frac{1}{2H} \mu_0 f(H) * m_{max} \nabla(\mathbf{H}^2) \quad (6)$$

Which is the same formula as used in section [2.2.1].

Appendix B: Supplementary to MATLAB simulations

B.1 Spread of magnetic moment

For determining the spread of magnetic moment of PC3-9 cells, a flow cytometry experiment was performed. First, PC3-9 cells were incubated with 5 $\mu\text{g}/\text{ml}$ of ferrofluids (CellSearch) for 3x10 min in a BD magnet array. Then, the sample is centrifuged and all unbound ferrofluids are aspirated. The cell pellet is then incubated with 5 $\mu\text{g}/\text{ml}$ goat anti-mouse IgG PE (Thermo Fisher Scientific, catalog # A10543) for 30 min at 37°C. This labels the ferrofluids with PE molecules. All unbound antibodies are washed away with centrifugation and the sample is then analyzed with a BD FACSAria II flow cytometer.

This resulted in Figure 1 below. As is visible in the flow cytometry histogram plot, there is quite a large spread in intensity, resulting to a large CV of roughly 220%.

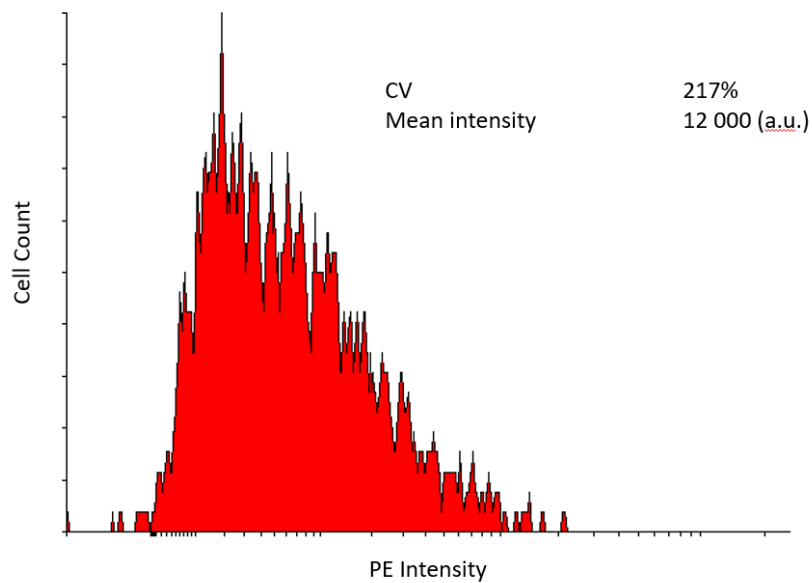


Figure 1: Flow Cytometry Histogram of PE intensities after staining PC3-9 cells with ferrofluids and anti-mouse IgG PE. The CV and mean intensities are both shown. Plot made with flowing software.

B.2. Modelling the magnetic field in COMSOL

To estimate the size of the magnetic field in the channel, COMSOL Multiphysics 5.3 was used. The Magnetic Fields, No Currents module can simulate permanent magnetic fields based on magnet orientation and a defined magnetization. An array of 3x20 mm magnets were simulated, with a 1160 kA/m magnetization which alternates in orientation. This resulted in Figure 2, which shows the gradient of the field.

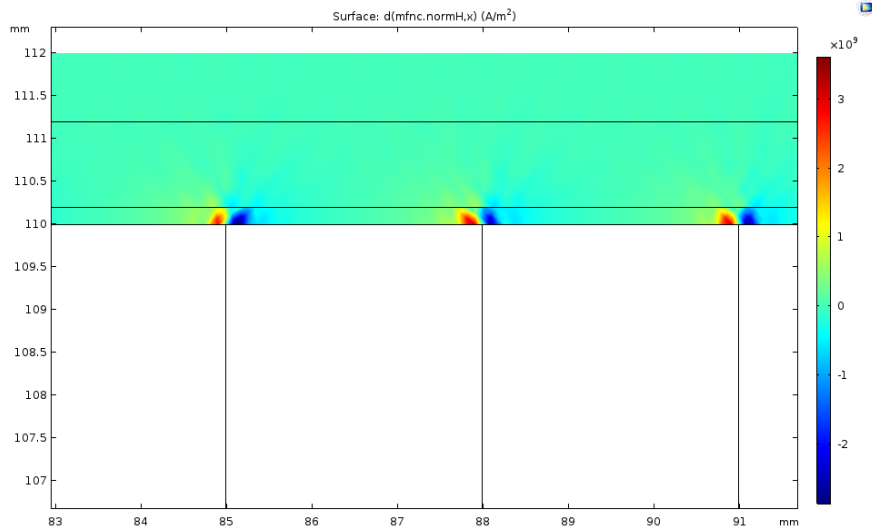


Figure 2: The magnetic field gradient as simulated with COMSOL.

The magnetic field was retrieved from COMSOL. To be able to estimate a value for each point on the channel height, the MATLAB function *fit* was used to create an exponential expression. This is shown in Figure 3.

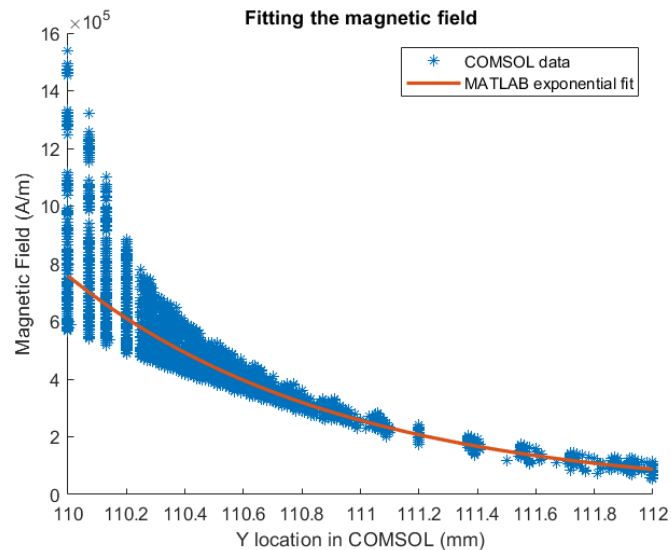


Figure 3: The magnetic field which is fitted in MATLAB.

Appendix C: validation of MATLAB based cell counting

To estimate whether the MATLAB script was able to accurately count cells, 15 images containing LNCAP cells stained by CellTracker Orange were counted both by the software as the student for validation. This showed a 95.2% accuracy of the software relative to the student, as visible in Table 1.

Photo	Count by software	Count by student	Deviation
1	8	8	0
2	5	6	1
3	5	5	0
4	26	26	0
5	11	12	1
6	3	3	0
7	6	6	0
8	9	9	0
9	6	7	1
10	3	3	0
11	14	16	2
12	5	5	0
13	6	6	0
14	18	19	1
15	13	14	1
Total	138	145	7
		Accuracy	95.2

Table 1: Validation of MATLAB cell counting script

Appendix D: Additional results to chapter 2

The complete table of PC3-9 recoveries of the experiment in which channel heights and flow rates were optimized, together with flow Reynolds numbers and average flow velocities is available in table 1. In Figure 1, an example of the flow cytometry plots is shown which was used for counting the different populations of cells used in the experiment of optimizing magnetic configuration.

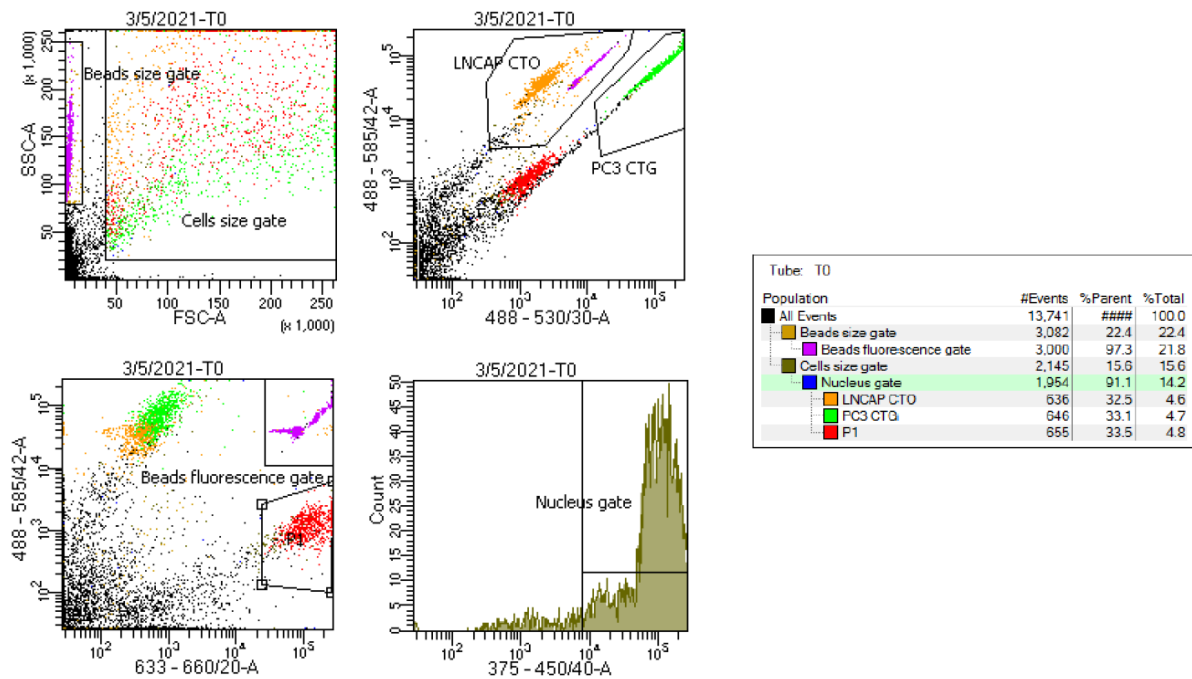


Figure 1: Flow Cytometry plots of one of the samples. Beads were gated for size and APC+ PE+ while the cells were gated on size, Nucleus and positivity for their respective dyes. Gate P1 represents the gate where PC3-9's were collected.

Flow rate (ml/min)	0.5	1	1.5	2
200 μm channel				
Flow speed (m/s)	0.0083	0.016	0.025	0.033
Flow Reynolds number medium	3.60	7.20	10.8	14.4
Capture rate 1 (%)	75	12	33	24
Capture rate 2 (%)	55	48	43	46
Capture rate 3 (%)	47	50	40	25
Average capture rate (%)	59.0	36.7	38.7	31.7
Standard deviation	11.8	17.5	4.2	10.1
400 μm channel				
Flow speed (m/s)	0.0041	0.0083	0.0125	0.016
Flow Reynolds number medium	3.46	6.93	10.40	13.8
Capture rate 1 (%)	70	40	60	30
Capture rate 2 (%)	73	60	33	42
Capture rate 3 (%)	53	27	37	36
Average capture rate (%)	65.3	42.3	43.3	36.0
Standard deviation	8.8	13.6	11.9	4.9
600 μm channel				
Flow speed (m/s)	0.0027	0.0055	0.0083	0.011
Flow Reynolds number medium	3.34	6.68	10.03	13.37
Capture rate 1 (%)	94	33	51	55
Capture rate 2 (%)	68	58	37	50
Capture rate 3 (%)	95	55	45	18
Average capture rate (%)	85.7	48.7	44.3	41.0
Standard deviation	12.5	11.1	5.7	16.4
800 μm channel				
Flow speed (m/s)	0.0021	0.0042	0.00625	0.0083
Flow Reynolds number medium	3.22	6.45	9.68	12.9
Capture rate 1 (%)	70	77	60	39
Capture rate 2 (%)	86	64	42	40
Capture rate 3 (%)	53	60	61	33
Average capture rate (%)	69.7	67.0	54.3	37.3
Standard deviation	13.5	7.3	8.7	3.1

Table 1: Results of testing the influence of flow rate and channel height on the recovery rate of PC3-9 cells incubated with 3.3 $\mu\text{g/ml}$ of Biomagnetic Solutions ferrofluid.